January 2019

Spectral Methods For Hamiltonian Systems And Their Applications

Lewei Zhao
Wayne State University, ZhaoleweiMath@gmail.com

Recommended Citation

SPECTRAL METHODS FOR HAMILTONIAN SYSTEMS AND THEIR APPLICATIONS

by

LEWEI ZHAO

DISSERTATION

Submitted to the Graduate School

of Wayne State University,

Detroit, Michigan

in partial fulfillment of the requirements

for the degree of

DOCTOR OF PHILOSOPHY

2019

MAJOR: APPLIED MATHEMATICS

Approved By:

_____

Advisor   Date

_____

_____

_____

DEDICATION

To My Family

ACKNOWLEDGEMENTS

Wuhan University. I appreciate for your help in discussions about applications of Hamiltonian systems in optimal control problems.

Finally, I would like to thank my sister, parents and grandparents. Thank for their selfless and endless support.

TABLE OF CONTENTS

LIST OF TABLES

LIST OF FIGURES

CHAPTER 1   INTRODUCTION

Sir William Rowan Hamilton originally introduced the Hamiltonian mechanics to describe the behavior of light, which was later further developed by Carl Gustav Jacob Jacobi. Hamiltonian systems have been seen to posses two remarkable properties : the solutions preserve the energy and the corresponding flow is symplectic ([1]). They have many applications in classical mechanics, molecular dynamics, astronomy, optimal control problems ([2]) and other scientific and engineering fields.

One step integrators that applied to Hamiltonian systems originate a transformation that is likewise canonical, which is useful in the long-time simulations. Kuntzmann ([3]) and Butcher ([4]) discovered that all s there exist Implict Runge-Kutta methods of order $2s$. To obtain the formulas of order $2s$, Butcher assumed the coefficients of the Gaussian quadrature formula. This implicit s-stage Gauss method of order $2s$ are symplectic for all s (Theorem 16.5 of [5]). After Feng Kang's enormous avalanche of research started on the characterization of Symplectic integration methods which preserve symplecticity and on the construction of new classes of symplectic methods ([6] to [10]). Suris ([11]) and Sanz-Serna ([12]) suggest the partitioned Runge-Kutta methods for separable Hamiltonian systems where it is possible to obtain explicit symplectic method. Geng Sun constructed several new classes of symplectic Runge-Kutta methods ([13]). One of his methods based on Radau quadrature. Also there are many other symplectic methods like Symplectic Nystrom Methods (II.16 of [5]), However the numerical solution of a symplectic integrator dose not share the energy preservation

property in general. Another disadvantage is most sympectic schemes are implicit and construction of higher order methods are quite complicated. ([14] is concerned with the finite element method for nonlinear Hamiltonian systems from conservation of energy, symplecticity and the global error.

A popular choice for constructing numerical approximation is using Spectral methods because of their attractive feature as geometric convergence rate under analytic assumption for the exact solution. There are already quite a few monographs/books about spectral methods ([15] and [16]). Three kinds of spectral methods (spectral Petrov-Galerkin, spectral collocation and spectral Galerkin methods) are analyzed in ([17]) for nonlinear Hamiltonian systems including the symplectic structure preserving properties, the energy and error estimates. By using those spectral schemes, the differential systems are discretized to algebraic equations which need to be solved by iteration. A good selection for initial value will greatly improve the computation efficiency. In this work we will propose two strategies to deal with initial value issues. For spectral collocation methods, we use existed scheme on a rough step size to calculate a approximated result as initial value. For spectral Galerkin method, we separate the system into linear part and nonlinear part. The solution to linear part is adopted as the initial value. A formulation for estimation of preserving energy error for general Hamiltonian system is set up by [17]. This work focus on a specific Hamiltonian system that the nonlinear part is polynomial and give more accurate estimation for its energy error by investigating the high order derivative of the Hamiltonian. A numerical example of the Henon-Helies system is shown to verify the linear accumulation of the

energy error.

Then we apply Spectral collocation methods and Spectral Galerkin methods to solving three types of problems : the first one is n-Body problem, which became one of the most celebrated problems in mathematics. The second one is Weyl's formula based on an effective confining potential. The last one is the optomechanical system, which can be used for quantum cooling. For n-Body problem, we simulate several interesting and important orbits in $\mathbb{R}^2$ including $n = 2, 3, 4$. For Weyl's law, an effective confining potential turns out to be a remarkable approximation of the density of states. We provide an approximation of the integrated density of states on a disk under inverse square potential. For exploring sideband cooling in optomechanical systems, we Then we propose an iterative algorithm and construct an appropriate set of basis functions such that the matrices in the discrete variational form are sparse. Finally, we provide some numerical experiments to show the efficiency of the algorithms. Moreover, we discuss a few new unsolved problems about nonsmooth Hamiltonian system.

CHAPTER 2 MATHEMATICS PROPERTIES OF THE HAMILTONIAN SYSTEMS

2.1 Definitions of The Hamiltonian Systems

In this section, we begin with some basic definitions and properties. We consider the system of Lagrange's equations ([18]) is equations

$$\dot{p} = \frac{\partial L}{\partial q} \tag{2.1.1}$$

where

$$p = \frac{\partial L}{\partial \dot{q}}$$

with a given Lagrangian function $L : \mathbb{R}^d \times \mathbb{R}^d \times \mathbb{R} \to \mathbb{R}$.

Example (Pendulum) Consider the mathematical pendulum in the homogeneous earth gravitational field. It consists of a weightless rigid straight arm of length l with one fixed end at 0 and a pointwise mass attached to the other end A.
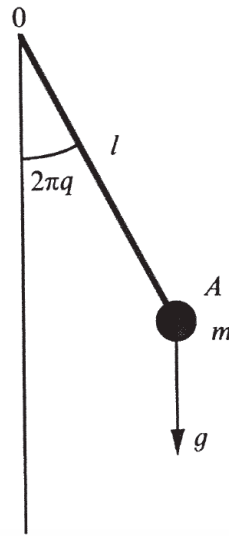
Figure 2.1.1: A pendulum in a homogeneous gravitional field

Take the angle variable $2\pi q$ which describes the deviation of the arm from the vertical stable position of the equilibrium. Then the Lagrangian of the system is given

by ([20])

$$L(q, \dot{q}) = 2\pi^2 ml^2 \dot{q}^2 + mgl \cos 2\pi q$$

From the Lagrangian function we obtain the Hamilton functions as

$$H(p, q) = p\dot{q} - L(q, \dot{q})$$

while L is a function of q and $\dot{q}$, H is a function of p and q.

Consequently $\dot{q}$ on the right hand side is a function of p and q. We obtain for the partial derivatives of H with respect to p and q the canonical equations

$$\frac{\partial H}{\partial p} = \dot{q} + p\frac{\partial \dot{q}}{\partial p} - \frac{\partial L}{\partial \dot{q}}\frac{\partial \dot{q}}{\partial p} = \dot{q}$$
$$\frac{\partial H}{\partial q} = p\frac{\dot{q}}{\partial q} - \frac{\partial L}{\partial q} - \frac{\partial L}{\partial \dot{q}}\frac{\partial \dot{q}}{\partial q} = -\dot{p}$$

(2.1.2)

Definition 2.1.1. *Hamiltonian system is a 2d dimensional ordinary differential equations for $i = 1, 2, ...d$,*

$$\dot{p}_i = -\frac{\partial H}{\partial q_i},$$
$$\dot{q}_i = \frac{\partial H}{\partial p_i}$$

(2.1.3)

Example A conservative Newtonian system

$$m_i \frac{d^2 q_i}{dt^2} = F_i(q_1, ..., q_d)$$

with

$$F_i(q) = -\frac{\partial V}{\partial q_i}$$

is of the form (2.1.3) if

$$H = \sum_{i=1}^{d} \frac{p_i^2}{2m_i} + V$$

Another example about spherical pendulum can be found in I.6 of [5].

Proposition 2.1.2. *The Hamiltonian system is equivalent to the system of Lagrange's*

equations ((2.1.1)).

Proof can be found in [18].

A Hamiltonian system can be rewritten as

$$z_t = -JH_z \tag{2.1.4}$$

where $H_z = (H_p, H_q)^T$ and $J = \begin{pmatrix} 0 & I_d \\ -I_d & 0 \end{pmatrix}$

A general form can be written as the gradient of flow driven by a free energy.

$$z_t = GH_z \tag{2.1.5}$$

A non-positive symmetric operator G gives the dissipation mechanism. Jie Shen etc.al recently proposed a new numerical technique called scalar auxiliary variable (SAV) approach to deal with nonlinear terms in a large class of gradient flow ([21], [22] and [23]).

2.2 Mathematical Background of the Hamiltonian Systems

As indicated in the following diagram, Hamiltonian theory operates in three different areas (variational principles, equations of motion and partial differential equations) which are all interconnected. Hamiltonian systems are characteristics equations of Hamilton-Jacobi equations (3.3 of [24]).

Hamiltonian Systems

Variational Principle $\longrightarrow$ Hamilton-Jacobi Equations
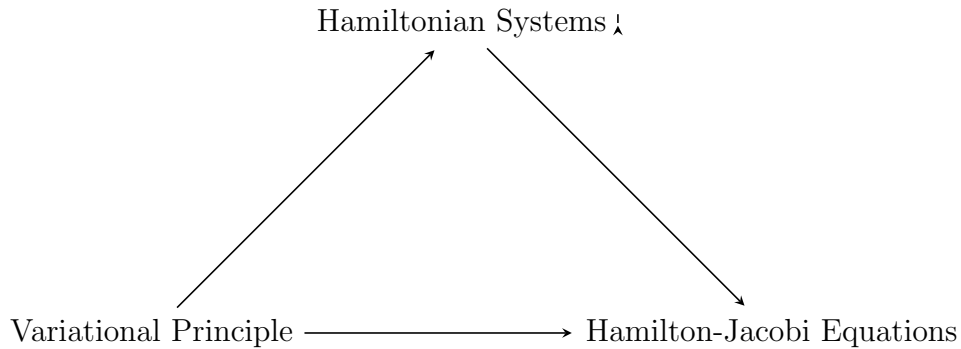
Hamilton-Jacobi equations ([25] and Chapter 10 of [24]) are very important in mechanics that can be generalized to Hamilton-Jacobi-Belleman equation, which has a lot of applications in equilibrium theory ([26]), portfolio choice problems in mathematical finance ([27],[28]) and optimal control theory ([29]). An overview of numerical methods for first-order Hamilton-Jacobi equations is given in [30].

2.3 Symplecticity

The study of Hamiltonian systems requires a detailed investigation of the underlying phase space with its intrinsic geometric structures. The main structure is the symplectic one.

A bilinear form g on a vector space V is called symplectic if it is nonsingular and skew-symmetric. The latter means $g(u, v) = -g(v, u)$ for any two vectors u and v. A pair (V, g) where V is a vector space and g is a symplectic form on V is called a symplectic vector space. A Hamiltonian mechanical system is given by an even-dimensional manifold, a symplectic structure on it ([18]).

Poincare introduced the following geometric point of view for differential equations.

Definition 2.3.1. *(Flow) For an autonomous system of differential equations.*

$$\dot{x} = f(x) \tag{2.3.1}$$

we define the flow $\varphi_t \colon \mathbb{R}^d \to \mathbb{R}^d$ to be the function which associates, for a given t, to the initial value $x_0 \in \mathbb{R}^d$ the corresponding solution value at time t,

$$\varphi_t(x_0) = x(t, 0, x_0)$$

For sets A of initial values we also study its behaviour under the action of the flow and write

$$\varphi_t(A) = \{x : x = x(t, 0, x_0), x_0 \in A\}$$

We can imagine, with Poincare, sets of molecules moving and being deformed with flow. Examples about transformation of sets under a flow can be found in I.14 of [5].

Theorem 2.3.2. *The flow of the Hamiltonian systems (2.1.3) preserves the volume.*

The author provides a new proof based on the theorem 14.8 in [5] which is rewritten as following lemma.

Lemma 2.3.3. *Consider the system (2.3.1) with continuously differentiable function $f(y)$. If tr(f'(y))=0 along the solution, the flow is volume-preserving, i.e, $Vol(\varphi_t(A)) = Vol(A)$.*

Then it is straight forward to check that $tr(H'(p, q)) = 0$ by

$$H'(p, q) = \begin{pmatrix} -\frac{\partial^2 H}{\partial p \partial q} & -\frac{\partial^2 H}{\partial q^2} \\ \\ \frac{\partial^2 H}{\partial p^2} & \frac{\partial^2 H}{\partial q \partial p} \end{pmatrix}$$

So theorem 2.3.2 is proved.

More general, we introduce the differential 2-form to represent the area.

$$\omega^2 = \sum_{i=1}^{d} dp_i \wedge dq_i$$
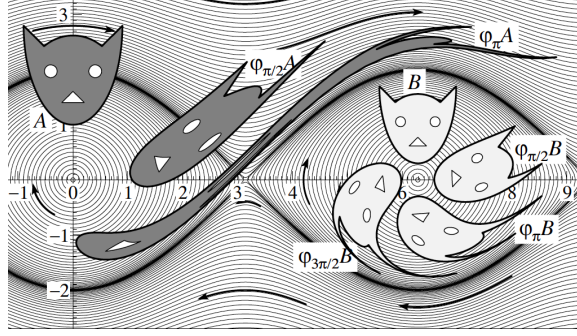
Figure 2.3.1: The flow of the pendulum systems preserves the areas (Fig2.2 of [19])

Definition 2.3.4. *(Symplectic) For a differentiable function $g: \mathbb{R}^{2d} \to \mathbb{R}^{2d}$ we define the differential form $g^*\omega^2$ by*

$$g^*\omega^2(\xi_1, \xi_2) = \omega^2(g'(p,q)\xi_1, g'(p,q)\xi_2)$$

Such a function g is called symplectic if

$$g^*\omega^2 = \omega^2$$

Proposition 2.3.5. *A linear symplectic map is injective.*

Proposition 2.3.6. *A differentiable transformation $g: \mathbb{R}^2 \to \mathbb{R}^2$ is symplectic if and only if its Jacobian $g'(p,q)$ satisfies*

$$g'^T J g' = J$$

with J given in (2.1.4)

More properties about symplectic structure can be found in [20].

Proposition 2.3.7. *The flow of the Hamiltonian systems* (2.1.3) *is symplectic.*

Proof can be found in [5] and [19]

2.4 Energy Conservation

Proposition 2.4.1. *The Hamiltonian function H is an first integral of the Hamiltonian system* (2.1.3), *i.e., H is a constant of motion : $H(p,q) = C$*

Proof can be found in Proposition 3.5 of [20].

CHAPTER 3 ALGORITHM AND ENERGY ERROR ESTIMATION

Spectral methods are one of most important approximation techniques for the computation of the solutions to differential equations, which are based on a polynomial expansion of the solution. The precision of the spectral methods is limited only by the regularity of the solution, in contrast to the finite element method and the finite difference methods.

We solve the system on [0,h] (for example h=1) first ,then use the obtained values (p(h),q(h)) as an initial condition to repeat the process on [h,2h] and so on......

In practice, we map the interval [kh,(k+1)h] to [-1,1] through the coordinate transform: $x = \frac{2}{h}t - (2k+1)$ and denote $P_i(x) = p_i(t)$, $Q_i(x) = q_i(t)$.

The transformed ODEs read

$$
\begin{aligned}
\dot{P}_i(x) &= -\frac{h}{2}\frac{\partial H}{\partial Q_i}, \\
\dot{Q}_i(x) &= \frac{h}{2}\frac{\partial H}{\partial P_i}
\end{aligned}
$$

(3.0.1)

3.1 Spectral Collocation Method

In practice, collocation methods (4.3 of [16], [32] and [33]) are usually employed. The concept of collocation is old and universal in numerical analysis. For ordinary differential equations it consists in searching for a polynomial of degrees whose derivative coincides (co-locates) at s given points with the vector field of the differential equation ([5]).

Definition 3.1.1. *(Collocation Method) For N a positive integer and c_i (i=1,....N) distinct real numbers, the corresponding collocation polynomial $u_N(x)$ of degree N is defined by*

$$
\begin{aligned}
\dot{u_N}(x_0 + c_i h) &= f(x_0 + c_i h, u_N(x_0 + c_i h)) \\
u_N(x_0) &= u_0
\end{aligned}
$$

(3.1.1)

The numerical solution is then given by

$$u_1 = u_N(x_0 + h) \tag{3.1.2}$$

The following conclusion states the relationship between collocation method and Runge-Kutta method.

Lemma 3.1.2. *(Guillou & Soule 1969, Wright 1970) The collocation method (3.1.2) is equivalent to the N-stage implicit Runge-Kutta method.*

$$k_i = f(x_0 + c_i h, u_0 + \sum_{j=1}^{N} a_{ij} k_j) \quad i = 1, ... N$$

$$u_1 = u_0 + h \sum_{i=1}^{N} b_i k_i \tag{3.1.3}$$

with coefficients

$$a_{ij} = \int_0^{c_i} l_j(t) dt, \quad b_j = \int_0^1 l_j(t) dt \tag{3.1.4}$$

where the $l_j(t)$ are the Lagrange polynomials

$$l_j(t) = \prod_{k \neq j} \frac{t - c_k}{c_j - c_k}$$

The proof can be found in [5] and [19].

For spectral collocation method, the collocation points $x_j = t_0 + c_j h$ are chosen as the zeros of orthogonal polynomials. For different types of orthogonal polynomials, we will have different kinds of spectral collocation method. For example, Jocobi collocation method is used in [34] to solve time-fractional Fokker-Planck equation.

3.1.1 Chebyshev Collocation Methods

In our current situation, it is natural to collocate at Chebyshev points. To define the Chebyshev points is in terms of the original angles ([31]) ,

$$x_j = cos(j\pi/N), \quad 0 \le j \le N$$

We interpolate P_i, Q_i as $P_{iN}(x) = \sum_{j=0}^{N} P_i(x_j)l_j(x), Q_{iN}(x) = \sum_{j=0}^{N} Q_i(x_j)l_j(x),$ where l_ji the Lagrange nodal basis function. We are seeking numerical approximations of $(P_i(x_j), Q_i(x_j))$, denote as (p_{ij}, q_{ij}). Since Chebyshev points are zeros of simple cos function, it has two remarkable advantages : one is convenient for implementing fast Fourier transform, the other one is the explicitly expression of the differentiation matrix $D = (d_{ij})_{i,j=0}^{N}$ with $d_{ij} = l_j'(x_i)$.

Proposition 3.1.3 (Chebyshev differentiation matrix, Theorem 7 in [35])**.** *For each* $N \ge 1$*, let the rows and columns of the* $(N+1) \times (N+1)$ *Chebyshev spectral differential matrix* D_N *be indexed from* 0 *to* N*. The entries of this matrix are*

$$(D_N)_{00} = \frac{2N^2 + 1}{6}, \quad (D_N)_{NN} = -\frac{2N^2 + 1}{6}$$

$$(D_N)_{jj} = -\frac{x_j}{2(1 - x_j^2)}, \quad j = 1, ..., N-1 \tag{3.1.5}$$

$$(D_N)_{ij} = \frac{(-1)^{i+i}c_i}{c_j(x_i - x_j)}, \quad i \ne j, \quad i, j = 0, ..., N$$

where

$$c_i = \begin{cases} 2, & i = 0 \quad or \quad N, \\ 1, & otherwise \end{cases}$$

The jth column of D_N contains the derivative of the degree N polynomial interpolant $p_j(x)$ to the delat function supported at x_j, sampled at the grid points x_i.Note that the rank of the $(N + 1) \times (N + 1)$ matrix D is N, we actually use the $D_N = (d_{ij})_{i,j=1}^{N}$.Therefore we solve the following system to obtain p_{iN}, q_{iN}.

$$F(p_{iN}, q_{iN}) = \begin{pmatrix} D_N & 0 \\ & \\ 0 & D_N \end{pmatrix} \begin{pmatrix} p_{iN} \\ \\ q_{iN} \end{pmatrix} + \frac{h}{2} \begin{pmatrix} \frac{\partial H}{\partial q}(p_{iN}, q_{iN}) \\ \\ -\frac{\partial H}{\partial p}(p_{iN}, q_{iN}) \end{pmatrix} + \begin{pmatrix} p_{i0}(d_{j0})_{j=1}^N \\ \\ q_{i0}(d_{i0})_{j=1}^N \end{pmatrix} \text{(3.1.6)}$$

We choose Newton Iteration Method to solve this system. Since Newton Method is sensitive to initial value, we use the existed symplectic scheme to get initial value on a rough time step. Note that the distribution of collocation points in [-1,1] is dense near the end and sparse in the centre. So we need to add some points in it. We select $\delta = \frac{1}{N}$, if distance between two adjacent points $h < \delta$, we do not add points. Otherwise we add $[\frac{h}{\delta}]$ equal-distance points. We denote the Jacobi matrix of F is J, the Newton iteration process is as following:

While $norm(dx) > 10^{-14}$
$dx = -J^{-1}F$;
$x_{n+1} = x_n + dx$;

Z.Zhang in [33] interprets the spectral collocation method at the Chebyshev points $x_j = cos(j\pi/N)$ as a Chebyshev-Galerkin method which is almost equivalent to (up to some higher-order terms) a Petrov-Galerkin method via the Chebyshev numerical integration (which is exact for polynomials of degree $\leq 2p - 1$), rather than the Clenshaw-Curtis quadrature (which is exact for polynomials of degree $\leq p$).

3.1.2 Symplecticity of Collocation Method

Next we are going to state the symplecticity preserving for the collocation method.

Definition 3.1.4. *(Symplectic Scheme) For a given Hamiltonian system, for a chosen one-step method (for example a Runge-Kutta method) and a choose step size h was*

denote by

$$\psi_h : \mathbb{R}^{2d} \quad \rightarrow \quad \mathbb{R}^{2d} \tag{3.1.7}$$

$$(p_n, q_n) \rightarrow (p_{n+1}, q_{n+1})$$

the transformation ψ is defined by the method. If ψ satisfies the symplecticity condition

$$(\frac{\partial(p_{n+1}, q_{n+1})}{\partial(p_n, q_n)})^T J \frac{\partial(p_{n+1}, q_{n+1})}{\partial(p_n, q_n)}) = J \tag{3.1.8}$$

then this method is a symplectic scheme.

Example: Verifying the Symplecticity of Two-Point Gauss Collocation Method for an Linear System.

Considering the Hamiltonian $H(p, q) = \frac{p^2 - q^2}{2}$

$$\begin{cases} \dot{p} = q \\ \dot{q} = p \end{cases}$$

The exact solution are

$$\begin{cases} p(t) = p(0)\cosh t + q(0)\sinh t \\ q(t) = p(0)\sinh t + q(0)\cosh t \end{cases}$$

This Hamiltonian system has no stable closed orbit but divergence. It still preserve the symplecticity :

$$\frac{\partial z}{\partial z_0} = [\begin{matrix} \cosh t & \sinh t \\ \sinh t & \cosh t \end{matrix}]$$

thus

$$(\frac{\partial z}{\partial z_0})^T J(\frac{\partial z}{\partial z_0}) = J$$

By two-points Gauss collocation method, choose collocation points :

$$s_0 = -1, s_1 = -\frac{\sqrt{3}}{3}, s_2 = \frac{\sqrt{3}}{3}$$

Let $l_i(x)$ be Lagrange basis functions at s_i as:

$l_0(x) = \frac{3x^2 - 1}{2}$, $l_1(x) = \frac{3+\sqrt{3}}{4}(1 - \sqrt{3}x)(x + 1)$, $l_2(x) = \frac{3-\sqrt{3}}{4}(\sqrt{3}x + 1)(x + 1)$

Their derivative as

$l_0'(x) = 3x$, $l_1'(x) = \frac{3+\sqrt{3}}{4}(1 - 2\sqrt{3}x - \sqrt{3})$, $l_2'(x) = \frac{3-\sqrt{3}}{4}(2\sqrt{3}x + \sqrt{3} + 1)$

Plug $x = s_i$ in (3.1.9)

$$
\begin{cases}
p_N'(x) = q_N(x) \\
q_N'(x) = p_N(x)
\end{cases}
\tag{3.1.9}
$$

We get a system of 6 equations

$$
\begin{cases}
p_N'(s_i) = q_i \\
q_N'(s_i) = p_i
\end{cases}
\tag{3.1.10}
$$

Simplified from (3.1.10) as :

$$
\begin{pmatrix} D_3 & -I_3 \\ -I_3 & D_3 \end{pmatrix} \begin{pmatrix} p_i \\ q_i \end{pmatrix} = 0
\tag{3.1.11}
$$

where

$$
D_3 = \begin{pmatrix}
-3 & \frac{3}{2} + \sqrt{3} & \frac{3}{2} - \sqrt{3} \\
-\sqrt{3} & \frac{3}{2} & \sqrt{3} - \frac{3}{2} \\
\sqrt{3} & -\frac{3}{2} - \sqrt{3} & \frac{3}{2}
\end{pmatrix}
\tag{3.1.12}
$$

Note that the rank of the D_3 is 2. Therefore, we may solve the system

$$
\begin{pmatrix}
\frac{3}{2} & \sqrt{3}-\frac{3}{2} & -1 & 0 \\
-\frac{3}{2}-\sqrt{3} & \frac{3}{2} & 0 & -1 \\
-1 & 0 & \frac{3}{2} & \sqrt{3}-\frac{3}{2} \\
0 & -1 & -\frac{3}{2}-\sqrt{3} & \frac{3}{2}
\end{pmatrix}
\begin{pmatrix}
p_1 \\ p_2 \\ q_1 \\ q_2
\end{pmatrix}
= \sqrt{3}
\begin{pmatrix}
p_0 \\ -p_0 \\ q_0 \\ -q_0
\end{pmatrix}
\tag{3.1.13}
$$

Then we solve for p_i and q_i

$$
\begin{cases}
p_1 = \dfrac{3(4-\sqrt{3})}{7}p_0 + \dfrac{9-4\sqrt{3}}{7}q_0 \\[2mm]
p_2 = \dfrac{3(4+\sqrt{3})}{7}p_0 + \dfrac{9+4\sqrt{3}}{7}q_0 \\[2mm]
q_1 = \dfrac{9-4\sqrt{3}}{7}p_0 + \dfrac{3(4-\sqrt{3})}{7}q_0 \\[2mm]
q_2 = \dfrac{9+4\sqrt{3}}{7}p_0 + \dfrac{3(4+\sqrt{3})}{7}q_0
\end{cases}
\tag{3.1.14}
$$

$$
\begin{cases}
p_N(1) = \displaystyle\sum_{i=0}^{2} p_i l_i(1) = p_0 + \sqrt{3}(p_2 - p_1) \\[2mm]
q_N(1) = \displaystyle\sum_{i=0}^{2} q_i l_i(1) = q_0 + \sqrt{3}(q_2 - q_1)
\end{cases}
\tag{3.1.15}
$$

Plug (3.1.14) in (3.1.15),

$$
\begin{cases}
p_N(1) = \dfrac{25p_0 + 24q_0}{7} \\[2mm]
q_N(1) = \dfrac{24p_0 + 25q_0}{7}
\end{cases}
\tag{3.1.16}
$$

$$
\frac{\partial z_N}{\partial z_0} = \frac{\partial(p_N(1), q_N(1))}{\partial(p_0, q_0)}
$$

thus calculation result as

$$
\left(\frac{\partial z_N}{\partial z_0}\right)^T J \left(\frac{\partial z_N}{\partial z_0}\right) = J
$$

which satisfies the symplectic condition (3.1.8).

The following result, discovered independently by at least three authors (F. Lasagni 1988, J.M. Sanz-Serna 1988, Y.B. Suris 1989) characterizes the class of all symplectic Runge-Kutta methods:

Lemma 3.1.5. *(Symplectic Runge-Kutta Methods) If the $N \times N$ matrix M with elements*

$$m_{ij} = b_i a_{ij} + b_j a_{ji} - b_i b_j, \quad i, j = 1, ..., N \tag{3.1.17}$$

satisfies $M = 0$, then Runge-Kutta method (3.1.3) is symplectic.

Proof can be found in [5].

For $N = 2$, let $t_0 = -1$ and $h = 2$ in (3.1.2), two Gauss collocation points are $x_1 = -\frac{\sqrt{3}}{3}$ and $x_2 = \frac{\sqrt{3}}{3}$.

then $c_1 = \frac{1}{2} - \frac{\sqrt{3}}{6}$ and $c_2 = \frac{1}{2} + \frac{\sqrt{3}}{6}$.

Plugging in(3.1.4), we have $a_{11} = a_{22} = \frac{1}{4}$, $a_{12} = \frac{3-2\sqrt{3}}{12}$, $a_{21} = \frac{3+2\sqrt{3}}{12}$

and $b_1 = b_2 = \frac{1}{2}$,

which satisfy the condition (3.1.17) in Lemma 3.1.5. This verifies that two-point collocation method is symplectic. In general, we have the symplecticity of the collocation method.

Theorem 3.1.6. *The collocation method (3.1.2) is symplectic.*

A systematic comparison of a spectral collocation method with some symplectic methods in solving Hamiltonian dynamical systems is conducted in [36]. And a general framework is introduced to convert a Spectral-Collocation method into a shooting-based variational integrator for Hamiltonian systems in [37].

3.2 Spectral-Galerkin Method

It is shown in [16] that the collocation method (3.1.2) with $\{x_j\}$ being the Jacobi-Gauss-Lobatto points, can be reformulated as a Galerkin method with numerical integration for second-order two-point boundary value problems in the case of homogeneous Dirichlet boundary conditions.

3.2.1 Algorithm description

Step 1: Introduce a suitable Sobolev space X and establish the weak form of the equations (3.0.1): Find $U_i(x) = (P_i(x), Q_i(x)) \in X$, such that

$$(\frac{dU_i(x)}{dx}, V_i) = (F_i(U_1, U_2, \cdots, U_n), V_i), \ \forall V_i \in X, \tag{3.2.1}$$

where $i = 1, 2, \cdots, d$.

Step 2: Define an approximation space $X_N = X \cap P_N$ and establish the discrete scheme corresponding to the weak form (3.2.1): Find $U_{iN}(x) \in X_N$, such that

$$(\frac{dU_{iN}(x)}{dx}, V_{iN}) = (F_i(U_{1N}, U_{2N}, \cdots, U_{dN}), V_{iN}), \ \forall V_{iN} \in X_N, \tag{3.2.2}$$

where $i = 1, 2, \cdots, d$ and P_N denotes the space of polynomial functions with a degree of no more than N on $[-1, 1]$.

Step 3: Establish an iterative algorithm corresponding to the discrete scheme (3.2.2): Find $U_{iN}^{k+1}(x) \in X_N$, such that

$$(\frac{dU_{iN}^{k+1}(x)}{dx}, V_{iN}) = (L_i(\mathbf{U}_N^{k+1}), V_{iN}) + (N_i(\mathbf{U}_N^k), V_{iN}) \ \forall V_{iN} \in X_N, \tag{3.2.3}$$

where $i = 1, 2, \cdots, d$, $\mathbf{U}_N^{k+1} = (U_{1N}^{k+1}, U_{2N}^{k+1}, \cdots, U_{dN}^{k+1})$, $\mathbf{U}_N^k = (U_{1N}^k, U_{2N}^k, \cdots, U_{dN}^k)$, $L_i(\mathbf{U}_N^{k+1})$ denote the linear part of $F_i(\mathbf{U}_N^{k+1})$ and $N_i(\mathbf{U}_N^k)$ denote the nonlinear part of $F_i(\mathbf{U}_N^k)$.

Step 4: Construct a set of appropriate basis functions $\varphi_0, \varphi_1, \cdots, \varphi_{N-1}$. Let

$$U_{iN}^{k+1} = \sum_{j=0}^{N-1} U_{i,j}^{k+1} \varphi_j \tag{3.2.4}$$

Now, plugging the expression of (3.2.4) in (3.2.3) and taking V_{iN} through all the basis functions in X_N, we will arrive at the following algebra systems:

$$\mathbf{QU}^{k+1} = \mathbf{F}^k, \tag{3.2.5}$$

where $\mathbf{Q}$ is the corresponding coefficient matrix.

Step 5: Set an iterative error accuracy *tol*, by using Matlab to repeatedly solve (3.2.5) until $\|\mathbf{U}^{k+1} - \mathbf{U}^k\|_{L^\infty} \leq tol$.

3.2.2 Legendre Polynomials Orthogonalization

Orthogonal Polynomials play a very important role in spectral interpolations. It is known that Legendre Polynomials ([15] and [38]) are set of orthogonal basis with L^2 norm over the interval $I = [-1, 1]$. In fact, it is a special case of Jacobi Polynomials, whose weight function is $\omega(x) = 1$.

In practice, we construct a set of basis functions for X_N. Let

$$\varphi_i(x) = L_i(x) - L_{i+2}(x)(i = 0, \cdots, N - 2), \varphi_{N-1}(x) = \frac{1}{2}(x + 1), \tag{3.2.6}$$

where $L_i(x)$ is the Legendre polynomial of degree i.

It is clear that

$$X_N = \text{span}\{\varphi_0(x), \cdots, \varphi_{N-2}(x), \varphi_{N-1}(x)\}.$$

Stiff matrix $s_{jk} = \int_{-1}^{1} \varphi_k' \varphi_j dx$ and mass matrix $m_{jk} = \int_{-1}^{1} \varphi_k \varphi_j dx$. Then it is known that

1. when $k, j = 0, 1, \cdots, N - 2,$

$$s_{jk} := \begin{cases} -2, & j = k + 1, \\ 2, & j = k - 1, \\ 0, & \text{other.} \end{cases} \quad m_{jk} = m_{kj} := \begin{cases} \frac{2}{2k+1} + \frac{2}{2k+5}, & j = k, \\ -\frac{2}{2k+5}, & j = k + 2, \\ 0, & \text{other.} \end{cases}$$

2. when $k = N - 1, j = 0, 1, \cdots, N - 2,$

$$s_{jk} = -s_{kj} =: \begin{cases} 1, & j = 0, \\ 0, & \text{other.} \end{cases} \quad m_{jk} = m_{kj} := \begin{cases} 1, & j = 0, \\ \frac{1}{3}, & j = 1, \\ 0, & \text{other.} \end{cases}$$

3. when $k = j = N - 1,$ $s_{kj} = \frac{1}{2}, m_{kj} = \frac{2}{3}.$

In summary, Spectral method is a global algorithm. We solve the system on each interval [kh,(k+1)h] globally. N usually is chosen as 20 or 30 can reach a very high accurate result. For finite element or finite difference method, the same precision need very small mesh or steps.

3.2.3   Symplectic up to a Spectral Accuracy

In this part, we will use the same notation as in [17]:

$z = (p_1, ..., p_d; q_1, ..., q_d)$ and $z_N = (p_{1N}, ..., p_{dN}; q_{1N}, ..., q_{dN})$

Proposition 3.2.1. *The spectral-Galerkin method is symplectic up to a sepctral accuracy, i.e.,*

$$\left(\frac{\partial z_N}{\partial z_0}\right)^T J\left(\frac{\partial z_N}{\partial z_0}\right) = J + O(e^{-\sigma N}) \tag{3.2.7}$$

where σ is some positive constant dependent on the regularity of the Hamiltonian function $H(z)$, and the error bound $e^{-\sigma N}$ is obtained from some Gauss or Gauss-Lobatto

numerical integration error.

Proof can be found in Theorem 2 of [17].

The error estimate of the algorithm of the spectral collocation and Galerkin method are established and proved that approximation error converges exponentially in [17].

3.3   Energy Error Estimation

The energy preserving properties of the collocation methods and spectral Galerkin methods on [-1,1] are studies in [17] presented as following theorem.

Proposition 3.3.1. *The Gauss spectral collocation method and Galerkin method is separately energy conserving up to a cell-average error and a Gauss numerical quadrature error. That is,*

$$H[z_N(1)] = H[z_N(-1)] + E_0$$

where E_0 is given in (3.4)-(3.5) in [17].

Zhimin Zhang proposed the main idea of the following theorem and its proof when he taught the course MAT 7270 Topics in Applied Mathematics in Fall 2015 at Wayne State University. This conclusion is stated as a remark in [17]. Here we emphasize the linear accumulation of the energy error by time and give the proof with detail.

Theorem 3.3.2. *(Linear Accumulation of the Energy Error)*

If a Hamiltonian system (2.1.3) is sufficiently smooth that

$$|\frac{d^{2N+1}}{dt^{2N+1}} H(p(t), q(t))| \leq C_N$$

then the energy error accumulated by time t for fixed N is

$$|H(p_N(T), q_N(T)) - H(p_N(0), q_N(0))| \leq \frac{(N!)^4}{(2N+1)[(2N)!]^3} C_N T$$

Proof. We interpolate p and q by $p_N(t) = \sum_{j=0}^{N} p_j \phi_j(t)$ and $q_N(t) = \sum_{j=0}^{N} q_j \phi_j(t)$ where ϕ_j is Lobatto basis. Spectral Method preserves energy approximately by $< \dot{H}(p_N, q_N), 1 >_N \approx \int_0^h \dot{H}(p_N, q_N) dt$ on [0,h].

And Gauss-Legendre Integration gives

$$
\begin{aligned}
< \dot{H}(p_N, q_N), 1 >_N &=< \frac{\partial H}{\partial p}(p_N, q_N)\dot{p_N}, 1 >_N + < \frac{\partial H}{\partial q}(p_N, q_N)\dot{q_N}, 1 >_N \\
&=< \frac{\partial H}{\partial p}(p_N, q_N), \dot{p_N} >_N + < \frac{\partial H}{\partial q}(p_N, q_N), \dot{q_N} >_N \\
&=< \dot{q_N}, \dot{p_N} >_N + < -\dot{p_N}, \dot{q_N} >_N \\
&= 0
\end{aligned}
\tag{3.3.1}
$$

Accurate integration $\int_0^h \dot{H}(p_N, q_N) dt = H(p_N(h), q_N(h)) - H(p_N(0), q_N(0))$

We want to estimate energy error on [0, T] and we choose h=1

$$
\begin{aligned}
|H(p_N(T), q_N(T)) - H(p_N(0), q_N(0))| &\leq \sum_{j=1}^{T} |H(p_N(j), q_N(j)) - H(p_N(j-1), q_N(j-1))| \\
&= \sum_{j=1}^{T} | \int_{j-1}^{j} \dot{H}(p_N, q_N) dt| \\
&= \sum_{j=1}^{T} | \int_{j-1}^{j} \dot{H}(p_N, q_N) dt - < \dot{H}(p_N, q_N), 1 >_N |
\end{aligned}
\tag{3.3.2}
$$

Corollary on Page 98 of [39] states that if $f \in C^{2N}[a, b]$, then

$\int_a^b f(x) dx - < f, 1 >_N = \frac{(b-a)^{2N+1}(N!)^4}{(2N+1)[(2N)!]^3} f^{(2N)}(\xi)$ where $a < \xi < b$.

So $| \int_{j-1}^{j} \dot{H}(p_N, q_N) dt - < \dot{H}(p_N, q_N), 1 >_N | \leq \frac{(N!)^4}{(2N+1)[(2N)!]^3} |H^{(2N+1)}(p_N(\xi_j), q_N(\xi_j))|$

Where $j - 1 < \xi_j < j$

Thus $|H(p_N(T), q_N(T)) - H(p_N(0), q_N(0))| \leq \frac{(N!)^4}{(2N+1)[(2N)!]^3} \sum_{j=1}^{T} |H^{(2N+1)}(p_N(\xi_j), q_N(\xi_j))|$

Where $j - 1 < \xi_j < j$

By smooth of Hamiltonian

$$
|H^{(2N+1)}(p_N(\xi_j), q_N(\xi_j))| < C_N
$$

Therefore, $|H(p_N(T), q_N(T)) - H(p_N(0), q_N(0))| \leq \frac{(N!)^4}{(2N+1)[(2N)!]^3} C_N T$ $\qquad\qquad\qquad\square$

.

Remark. **3.1** By Stirling's Formula

$$\frac{(N!)^4}{(2N+1)[(2N)!]^3} \sim \frac{e^{2N}\sqrt{\pi}}{(2N+1)2^{6N+1}N^{2N-\frac{1}{2}}}$$

For N=20, $\frac{(N!)^4}{(2N+1)[(2N)!]^3} \approx 1.5732 \times 10^{-72}$

For N=30, $\frac{(N!)^4}{(2N+1)[(2N)!]^3} \approx 1.4086 \times 10^{-118}$

Remark. **3.2**

$$H^{(2N+1)}(p_N(\xi_j), q_N(\xi_j)) = \sum_{k=0}^{N} \binom{2N}{k}[\dot{q}^{(2N-k)}(p_N, q_N)\dot{p_N}^{(k)} - \dot{p}^{(2N-k)}(p_N, q_N)\dot{q_N}^{(k)}]$$

3.3.1 Energy Error for Hamiltonian Systems with Polynomial Nonlinear Part

Definition 3.3.3. *Define the 1-norm of the coefficient vector for a polynomial $P_N(x) = \sum_{n=0}^{N} a_n x^n$ as*

$$\|P_N(x)\|_1^* = \sum_{n=0}^{N} |a_n|$$

Lemma 3.3.4. *For $n = 2N + 1, 2N + 2,...,M$, we have*

$$\frac{n!}{(n-2N-1)!} \leq \frac{M!}{(M-2N-1)!} \tag{3.3.3}$$

Proof. We prove it by induction for n when $n = M$ it is correct, we assume $n = M - k$ is correct, then for $n = M - k - 1$

$$\frac{n!}{(n-2N-1)!}$$

$$=\frac{(M-K-1)!}{(M-k-2N-2)!}$$

$$=\frac{(M-k)!}{(M-k-2N-1)!}\frac{M-K-2N-1}{M-K} \quad (3.3.4)$$

$$\leq\frac{(M-k)!}{(M-k-2N-1)!}$$

$$\leq\frac{M!}{(M-2N-1)!}$$

by introduction it is proved. $\qquad\square$

Theorem 3.3.5. *For a Hamiltonian system* (2.1.3) *with* $H(p,q)=\sum p^i q^j$ *(d=1), then the energy error accumulated by time T for fixed N is*

$$|H(p_N(T),q_N(T))-H(p_N(0),q_N(0))| \leq \frac{(N!)^4 T}{(2N+1)[(2N)!]^3}\sum_{i+j>2}\frac{[(i+j)N]!}{[(i+j-2)N-1]!}\|p_N^i q_N^j\|_1^*$$

where $\| \quad \|_1^*$ *is 1-norm of the coefficient vector.*

Proof.

$$|H^{(2N+1)}(p_N(\xi_j),q_N(\xi_j))| = |\sum_{i+j>2} p_N^i q_N^j(\xi_j))^{(2N+1)}| \quad (3.3.5)$$

Let $p_N^i q_N^j(t) = \sum_{n=0}^{(i+j)N} b_n t^n$, then by Lemma 3.3.3,

$$|p_N^i q_N^j(t))^{(2N+1)}| = |\sum_{n=2N+1}^{(i+j)N}\frac{n!}{(n-2N-1)!}b_n t^{n-2N-1}|$$

$$\leq \frac{[(i+j)N]!}{[(i+j-2)N-1]!}\sum_{n=2N+1}^{(i+j)N}|b_n| \quad (3.3.6)$$

$$\leq \frac{[(i+j)N]!}{[(i+j-2)N-1]!}\|p_N^i q_N^j\|_1$$

Then we apply the (3.3.6) to Theorem 3.3.1 and (3.3.5), we got the estimation.

$\qquad\square$

This theorem can be straightforward generalized to any dimension d.

3.4   Numerical Validation : Henon-Heiles System

Consider the Henon-Heiles System

$$H(p_1, p_2, q_1, q_2) = \frac{1}{2}(p_1{}^2 + p_2{}^2 + q_1{}^2 + q_2{}^2) + q_1{}^2 q_2 - \frac{1}{3}q_2{}^3$$

Its nonlinear Hamiltonian is a polynomial. The corresponding system of nonlinear ODE for this H is

$$
\begin{aligned}
\dot{p}_1(t) &= -\frac{\partial H}{\partial q_1} = -q_1 - 2q_1 q_2 \\
\dot{p}_2(t) &= -\frac{\partial H}{\partial q_2} = -q_2 - q_1{}^2 + q_2{}^2 \\
\dot{q}_1(t) &= \frac{\partial H}{\partial p_1} = p_1 \\
\dot{q}_2(t) &= \frac{\partial H}{\partial p_1} = p_1
\end{aligned}
\tag{3.4.1}
$$

First we can do a little theoretic analysis about the system. There are 4 four equilibrium points for this system which are $E_1 = (0, 0, 0, 0)$, $E_2 = (0, 0, 0, 1)$, $E_3 = (0, 0, \frac{\sqrt{3}}{2}, -\frac{1}{\sqrt{2}})$, $E_4 = (0, 0, -\frac{\sqrt{3}}{2}, -\frac{1}{\sqrt{2}})$

The Hessen Matrix of H is

$$
D^2 H = \begin{pmatrix}
1 & 0 & 0 & 0 \\
0 & 1 & 0 & 0 \\
0 & 0 & 1 + 2q_2 & 2q_1 \\
0 & 0 & 2q_1 & 1 - 2q_2
\end{pmatrix}
$$

Buy judging it is positive , negative or neither, we can know E_1 is a local maximal point and others are saddle points. With the help of graph of contour plot of energy H in [36] , we know there are 3 exits for the energy to escape according to the 3 saddle points. The total energy H=0 for E_1 and $H = \frac{1}{6}$ for E_1, E_2, E_3. If the initial energy is far beyond this H, the particles wander inside the region for a certain time in the

scattering region until they cross one of the three energy line and escape to infinity. That is to say, when the initial $H < \frac{1}{6}$, the solution is regular; when $H > \frac{1}{6}$, the solution is chaotic. Note that the time they spent in bounded region is named " escape time ". If the energy is higher, then the escape time is shorter.

we use the explicit symplectic scheme of order 2 in [36] as following to get initial value.

$$
\begin{aligned}
p_1{}^{k+1} &= p_1{}^k - \frac{h}{2}(q_1{}^k + 2q_1{}^k q_2{}^k) \\
p_2{}^{k+1} &= p_2{}^k - \frac{h}{2}(q_2{}^k + q_1{}^{k^2} - q_2{}^{k^2}) \\
q_1{}^{k+1} &= q_1{}^k - \frac{h}{2}p_1{}^{k+1} \\
q_2{}^{k+1} &= q_2{}^k - \frac{h}{2}p_2{}^{k+1}
\end{aligned}
\tag{3.4.2}
$$

Note that the distribution of collocation points in [-1,1] is dense near the end and sparse in the centre. So we need to add some points in it. We select $\delta = \frac{1}{N}$, if distance between two adjacent points $h < \delta$, we do not add points. Otherwise we add $[\frac{h}{\delta}]$ equal-distance points.

We select two different sets of initial conditions. The first set represents a regular case with initial condition

$$p_1(0) = 0.011, p_2(0) = 0, q_1(0) = 0.013, q_2(0) = -0.4$$

In this case, $H_0 = 0.101410733 < \frac{1}{6}$

The second set is a chaotic case with

$$p_1(0) = \sqrt{2 \times 0.15925}, p_2(0) = q_1(0) = q_2(0) = 0.12$$

In this case, $H_0 = 0.182002 > \frac{1}{6}$.

Figure 3.4.2 shows the chaotic solution by spectral collocation N=20 and the phase plot when the particle wanders in the bounded region until it crosses the energy thresh-
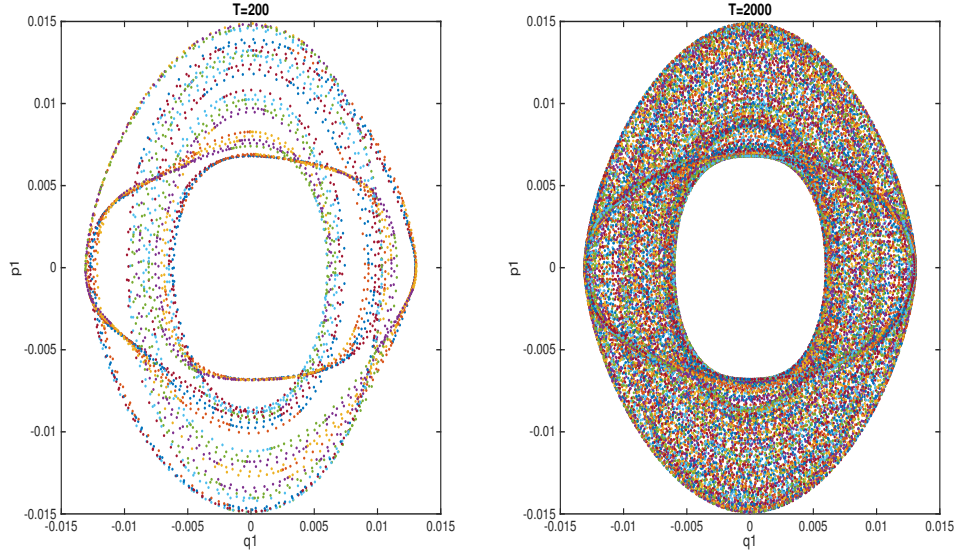
Figure 3.4.1: Phase plots of a regular solution by collocation $N = 20$.

old line and escapes. The first one is on [0,24] and the other one is phase plot q_2 versus q_1 on [0,24]. When $T > 24$, it will convergent very slowly.

The error in energy H,and the CPU times are presented in the table. We choose initial conditions from the regular case when N=20. The CPU times used are much less than [36].

Theorem 3.3.4 gives energy error estimate that

$$|H(p_N(T), q_N(T)) - H(p_N(0), q_N(0))| \leq \frac{(N!)^4(3N)!T}{(2N+1)[(2N)!]^3(N-1)!}(\|p_{1,N}^2 q_{2,N}\|_1^* + \frac{1}{3}\|q_{2,N}^3\|_1^*)$$

which is verified by Figure 3.4.3 and Table 3.4.1.
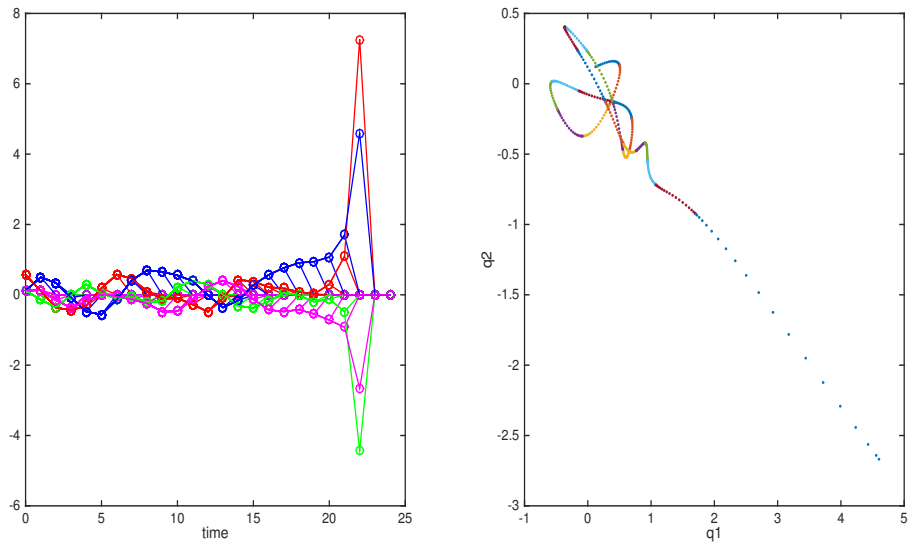
Figure 3.4.2: Phase plots of a chaotic solution by collocation $N = 20$ for T=24.
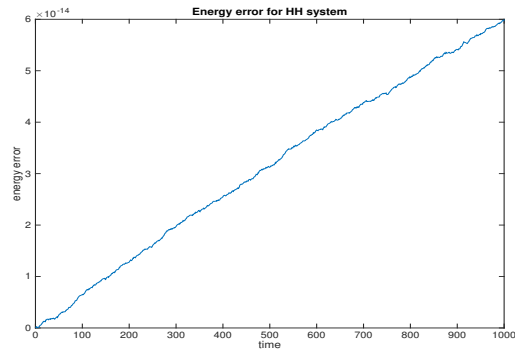
Figure 3.4.3: Energy error linearly accumulated

T	time(secs)	Error in Energy
[0,1000]	3	5.5345×10^{-14}
[0,10^4]	21	5.6853×10^{-13}
[0,10^5]	232	5.8277×10^{-12}
[0,10^6]	2234	5.8806×10^{-11}

Table 3.4.1: The energy loses as linear as losing 10^{-14} every period t=1000.

Collacation on [0,10]
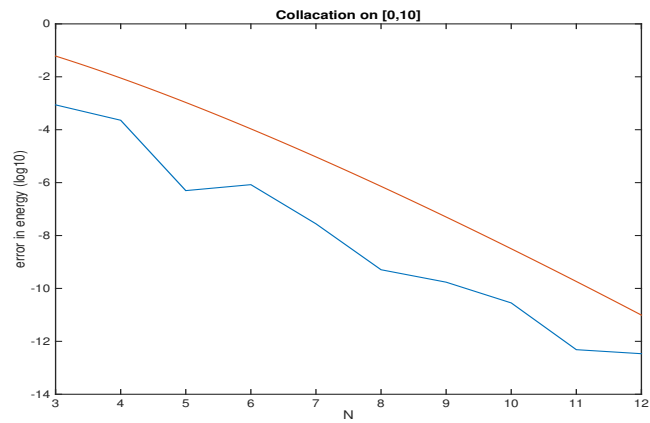
Figure 3.4.4: The rate of convergence in energy on [0,10]

Using the regular initial values is shown in the figure 3.4.4, Spectral Collocation gives the rate in the order of $\left(\frac{1}{N}\right)^{0.85N}$.

CHAPTER 4   APPLICATION I: N-BODY PROBLEMS IN TWO DIMENSIONS

In this section, we shall consider n point masses moving in a Newtonian reference system $\mathbb{R}^2$ with the only force acting on them being their mutual gravitational attraction.

Considering $4n$ dimensional Hamiltonian $H(p,q) = \frac{1}{2}\sum_{i=1}^{n} m_i(p_{ix}^2 + p_{iy}^2) - \sum_{1 \le i < j \le n} \frac{m_i m_j}{|q_i - q_j|}$, where $|q_i - q_j| = \sqrt{(q_{ix} - q_{jx})^2 + (q_{iy} - q_{jy})^2}$.

$$
\begin{cases}
\dot{p}_{ix} = \sum_{j \ne i} \dfrac{m_j(q_{jx} - q_{ix})}{|q_j - q_i|^3} \\[2mm]
\dot{p}_{iy} = \sum_{j \ne i} \dfrac{m_j(q_{jy} - q_{iy})}{|q_j - q_i|^3} \\[2mm]
\dot{q}_{ix} = m_i p_{ix} \\[2mm]
\dot{q}_{iy} = m_i p_{iy}
\end{cases}
\tag{4.0.1}
$$

4.1   A Modified Two-Body Problems

Celestial mechanics as we know today started with Newton's formulations of the three laws of motion, the universal law of gravity, and its solution of the two-body problem. The Kepler two-body problem describes the motion of two bodies under mutual gravitational attraction.The sun and one planet can be considered as a 2-body problem. A modified problem is the Hamiltonian System ([40]) with

$$
H(p_1, p_2, q_1, q_2) = \frac{1}{2}(p_1^2 + p_2^2) - \frac{1}{\sqrt{q_1^2 + q_2^2}} - \frac{\epsilon}{2\sqrt{(q_1^2 + q_2^2)^3}}
$$

where ϵ is a small perturbation parameter.

The corresponding system of nonlinear ODE for this H is

$$\dot{p}_1(t) = -\frac{\partial H}{\partial q_1} = -\frac{q_1}{\sqrt{(q_1^2 + q_2^2)^3}} - \frac{3\epsilon q_1}{2\sqrt{(q_1^2 + q_2^2)^5}}$$

$$\dot{p}_2(t) = -\frac{\partial H}{\partial q_2} = -\frac{q_2}{\sqrt{(q_1^2 + q_2^2)^3}} - \frac{3\epsilon q_2}{2\sqrt{(q_1^2 + q_2^2)^5}}$$

$$\dot{q}_1(t) = \frac{\partial H}{\partial p_1} = p_1 \tag{4.1.1}$$

$$\dot{q}_2(t) = \frac{\partial H}{\partial p_2} = p_2$$

This is a modification of the two-body problem. It is about the system of two massive bodies that attract each other by the gravitational force. The first body is located at the origin. This model describes the motion of a particle in a plane. A particle in this model is attracted gravitationally by a slightly oblate sphere instead of a point mass. We use Chebyshev-Guass-Lobatto Collocation Method to solve it. Initial value are calculated by the Störmer-Verlet Scheme in page 7 of [19] as following

$$p_1^{k+\frac{1}{2}} = p_1^k - \frac{h}{4}\left(\frac{q_1^k}{\sqrt{(q_1^k + q_2^k)^3}} + \frac{3\epsilon q_1^k}{2\sqrt{(q_1^k + q_2^k)^5}}\right)$$

$$p_2^{k+\frac{1}{2}} = p_2^k - \frac{h}{4}\left(\frac{q_2^k}{\sqrt{(q_1^k + q_2^k)^3}} + \frac{3\epsilon q_2^k}{2\sqrt{(q_1^k + q_2^k)^5}}\right)$$

$$q_1^{k+1} = q_1^k + \frac{h}{2}p_1^{k+\frac{1}{2}}$$

$$q_2^{k+1} = q_2^k + \frac{h}{2}p_2^{k+\frac{1}{2}} \tag{4.1.2}$$

$$p_1^{k+1} = p_1^{k+\frac{1}{2}} - \frac{h}{4}\left(\frac{q_1^{k+1}}{\sqrt{(q_1^{k+1} + q_2^{k+1})^3}} + \frac{3\epsilon q_1^{k+1}}{2\sqrt{(q_1^{k+1} + q_2^{k+1})^5}}\right)$$

$$p_2^{k+1} = p_2^{k+\frac{1}{2}} - \frac{h}{4}\left(\frac{q_2^{k+1}}{\sqrt{(q_1^{k+1} + q_2^{k+1})^3}} + \frac{3\epsilon q_2^{k+1}}{2\sqrt{(q_1^{k+1} + q_2^{k+1})^5}}\right)$$

we choose step size $h = 1$. Besides the energy H, this system also preserves the angular momentum which is $q_1 p_2 - p_1 q_2$. The numerical result for preserving energy and angular momentum are better than [36] under guessed initial value as well as CPU time used. Figure 4.1.1 and Table 4.1.1 show the structure preserved of this problem.
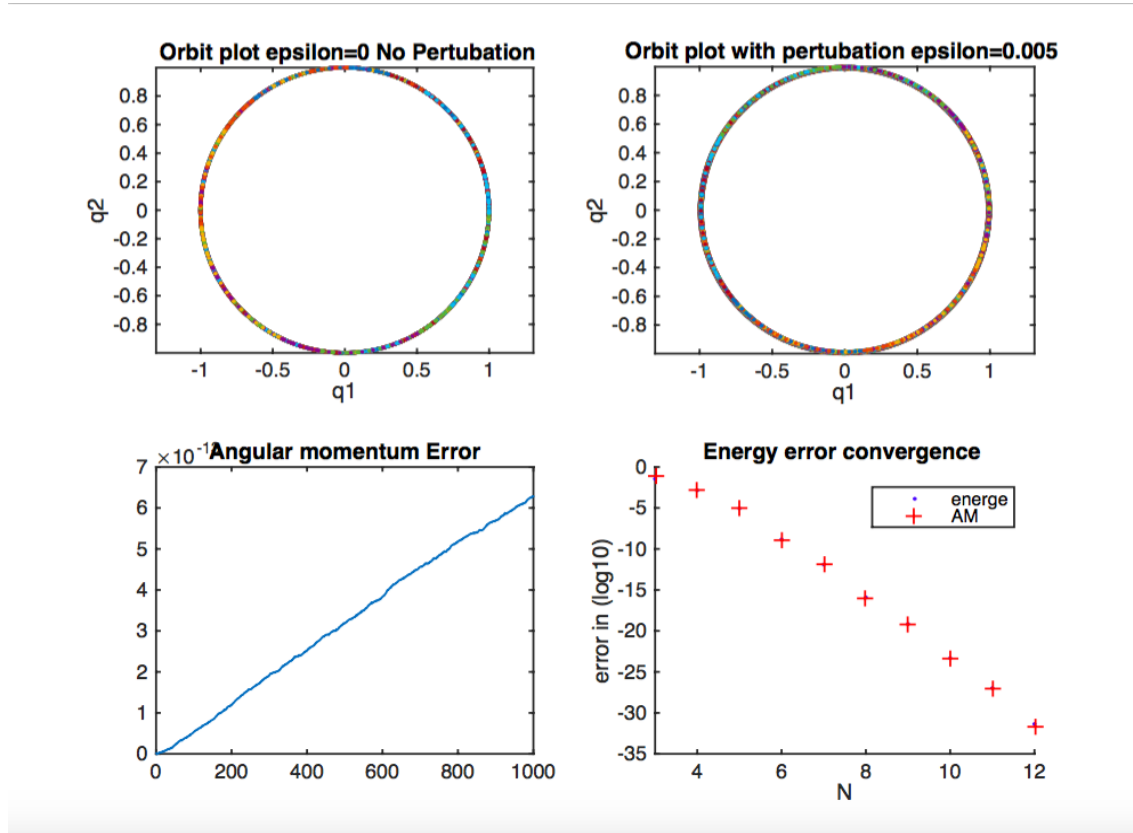
Figure 4.1.1: T=1000 with $N = 20$ of modified two-body problems under the initial condition $p_1(0) = q_2(0) = 0, p_2(0) = \sqrt{\frac{1+e}{1-e}}, q_1(0) = 1 - e$ (eccentricity e=0.001)

T	time(secs)	Error in Energy	Error in Angular Momentum
$[0,1000]$	26	6.376×10^{-13}	6.2816×10^{-13}
$[0,10^4]$	1807	6.3745×10^{-12}	6.2786×10^{-12}

Table 4.1.1: Comparison when $N = 20, \epsilon = 0.005$ with initial condition $p_1(0) = q_2(0) = 0, p_2(0) = \sqrt{\frac{1+e}{1-e}}, q_1(0) = 1 - e(e = 0.001)$. The Newton iteration needs 5 times at each step
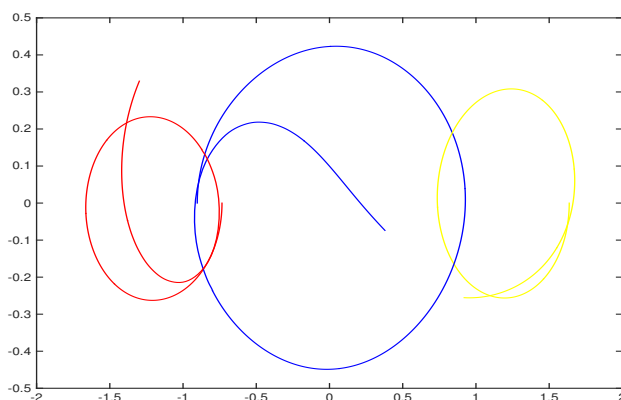
Figure 4.2.1: T=6 of 3-body Brocke-Hennon Orbit, error of Hamiltonian is 0.245 with $N = 20$ under the initial condition $p_{ix}(0) = -0.003$, $p_{1y} = 2.4654$, $p_{2x} = 0.003$, $p_{2y} = -2.2444$, $p_{3y} = -0.221$, $q_{1x} = -0.9029$, $q_{2x} = -0.7341$, $q_{3x} = 1.637$ and $p_{3x} = q_{iy} = 0$.

4.2 Three-Body Problems

Newton then turned his attention to the motion of the moon, which requires three bodies: the sun, earth and the moon.

4.2.1 Brocke-Henon Orbit

An one-parameter family of periodic orbits in the planar equal-mass three-body problem was found numerically by Henon, in which the angular momentum is chosen as the non-trivial parameter. There is a special orbit in this family as shown in Fig.4.2.1, which has a simple shape and good symmetry properties. This orbit was also independently discovered by Broucke and it is called as the Broucke-Henon orbit ([41]). Simulation of this orbit by spectral method is given in Figure 4.2.1.
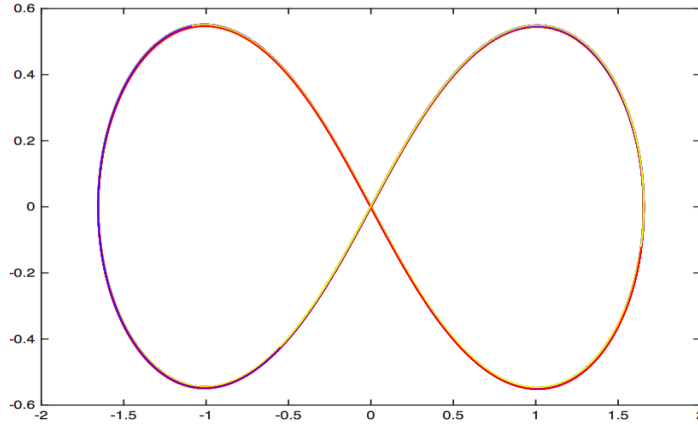
Figure 4.2.2: T=500 of 3-body Figure Eight, error of Hamiltonian is 9.6916×10^{-12} with $N = 20$ under the initial condition $p_{1x}(0) = p_{3x}(0) = 0.3765$, $p_{1y} = p_{3y} = 0.3492$, $p_{2x} = -0.7530$, $p_{2y} = -0.6984$, $q_{1x} = -q_{3x} = 1.4861$, $q_{1y} = -q_{3y} = -0.3724$ and $q_{2x} = q_{2y} = 0$.

4.2.2 Figure Eight Orbit

Definition 4.2.1. *A simple choreographic solution is a periodic solution that all bodies chase one another along a single closed orbit.*

Many relative equilibria cause simple choreographic solutions and they are called trival choreographic solutions (circular motions). The first remarkable non-trivial chore-graphic solution Figure Eight was first discovered numerically by Cristopher Moore in [42]. The orbit has 0 angular momentum and a very rich symmetry pattern ([43]). Linear stability of the Eight solution restricted to the plane are numerically proved by multiple precision interval arithmetic in [44] and shown by using symmetry reduction in [45]. Figure 4.2.2 shows a simulation of this Eight shape orbit.

4.3 Four-Body Problems

We consider the boundary value problem with boundary configurations in [46] as following :

$$q(0) = \begin{pmatrix} a_1 & a_2 \\ 0 & -a_3 \\ -a_1 & a_2 \\ 0 & a_3 - 2a_2 \end{pmatrix}, \quad q(T) = \begin{pmatrix} -a_5 & a_4 \\ a_5 & a_4 \\ -a_6 & -a_4 \\ a_6 & -a_4 \end{pmatrix} \begin{pmatrix} \cos\theta & -\sin\theta \\ \sin\theta & \cos\theta \end{pmatrix} \tag{4.3.1}$$

that $q(0)$ forms an isosceles triangle with one in the axis of the triangle and $q(T)$ forms a trapezoid. Then we use the following shooting method to solve $p(0)$:

System (4.0.1) for $n = 4$ can be written as a second order ODE

$$\frac{d^2}{dt^2} \begin{pmatrix} q_{ix} \\ q_{iy} \end{pmatrix} = \sum_{j \neq i} \begin{pmatrix} \frac{q_{jx} - q_{ix}}{|q_j - q_i|^3} \\ \frac{q_{jy} - q_{iy}}{|q_j - q_i|^3} \end{pmatrix} \tag{4.3.2}$$

Let

$$p(0) = s = \begin{pmatrix} s_{1x} & s_{1y} \\ s_{2x} & s_{2y} \\ s_{3x} & s_{3y} \\ s_{4x} & s_{4y} \end{pmatrix} \tag{4.3.3}$$

Differentiate (2.3.1), $q(0)$ in (4.3.1) and (4.3.3) with respect to s

$$\begin{cases} \dfrac{d^2}{dt^2} D_s \begin{pmatrix} q_{ix} \\ \\ q_{iy} \end{pmatrix} = \sum_{j \neq i} D_q \begin{pmatrix} \dfrac{q_{jx}-q_{ix}}{|q_j-q_i|^3} \\ \\ \dfrac{q_{jy}-q_{iy}}{|q_j-q_i|^3} \end{pmatrix} D_s q \\ \\ D_s q(0) = 0 \\ \\ D_s p(0) = I_8 \end{cases} \tag{4.3.4}$$

We summarize the shooting algorithm as following :

Given s_n, solve 32-dimensional ODE

$$\begin{cases} \dot{p}_i = \sum_{j \neq i} \dfrac{q_j - q_i}{|q_j - q_i|^3} \\ \\ \dot{D_s p_i} = \sum_{j \neq i} D_q \dfrac{q_j - q_i}{|q_j - q_i|^3} D_s q \\ \\ \dot{q}_i = p_i \\ \\ \dot{D_s q_i} = D_s p_i \end{cases} \tag{4.3.5}$$

with initial value

$$\begin{cases} p(0) = s_n \\ \\ D_s p(0) = I_8 \\ \\ D_s q(0) = 0 \end{cases} \tag{4.3.6}$$

and $q(0)$ is given by (4.3.1),

then by Newton's iteration,

$$s_{n+1} = s_n - D_s q(T; s_n)^{-1} [q(T; s_n) - q(T)]$$

we get $p(0)$ thus convert the boundary problem into initial value problem as before.
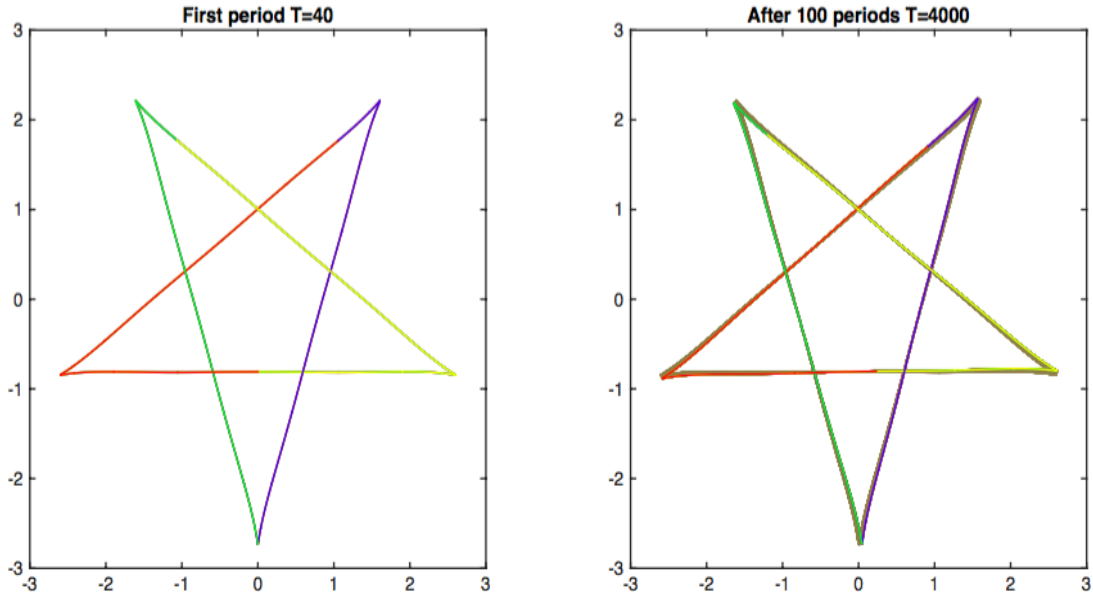
Figure 4.3.1: 1st body's orbit of the 4-body Problem , error of the Hamiltonian is 6.6613×10^{-16} for the first minimal period T=40 and 4.498×10^{-13} after 100 periods ($N = 20$).

4.3.1 Stable Simple Choreographic Orbits

A rigorous proof of the existence of infinitely many simple choregraphic solutions in the classical Newtonian 4-body problem is given in [46]. Among the many linearly stable simple choreographic orbits, the star pentagon is one of the most extraordinary choreographic solution which was found by [46]. In (4.3.1), let $T = 1$ and $\theta = \frac{2\pi}{5}$ and a_i (i=1,...,6) are given in Fig.1 of [46]. By assembling out the initial four pieces of curves from $q(0)$ to $q(T)$, a star pentagon is formed (Figure 4.3.1). A perturbation of the star pentagon orbit is illustrated in Figure 4.3.2.

All initial condition below for 4-body problems are chosen from Appendix C in [46]. An example of another simple choreographic orbits for 4 body problem is shown in Figure 4.3.3.
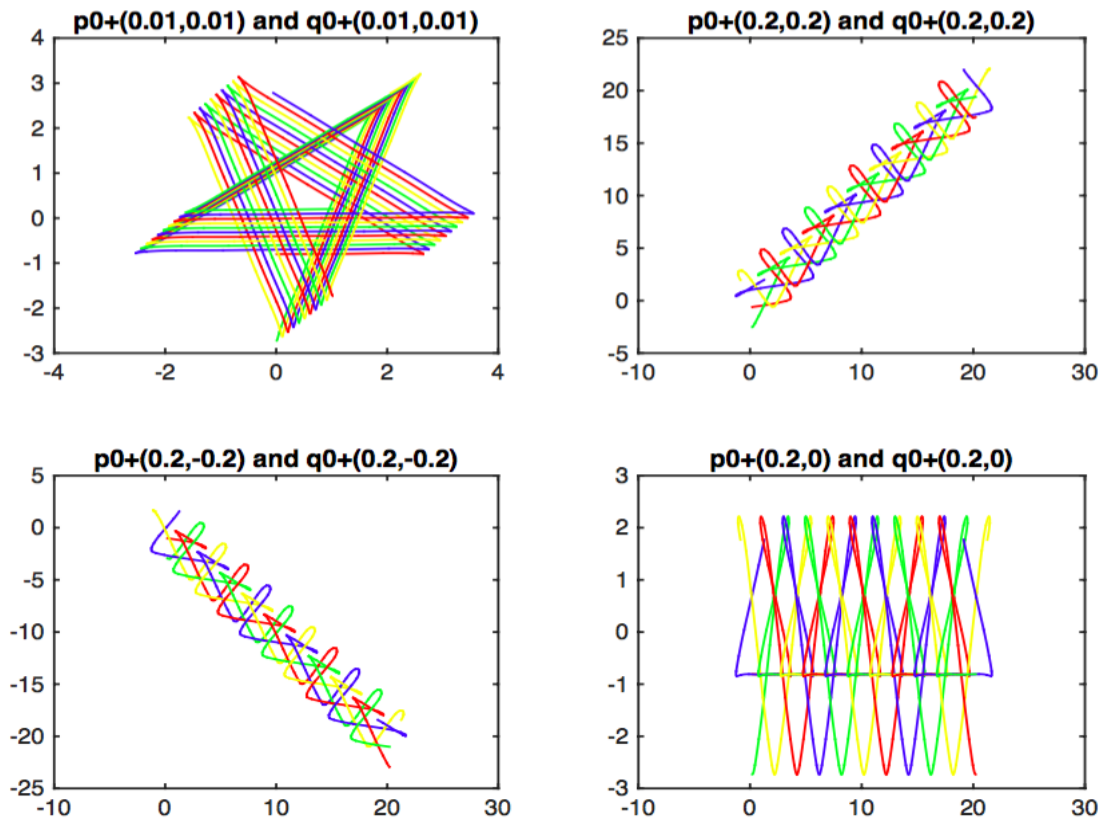
Figure 4.3.2: T=100 of 4-body Star Pentagon Orbit under the perturbation in different intensity and angles. The energy is still preserved with $N = 20$.
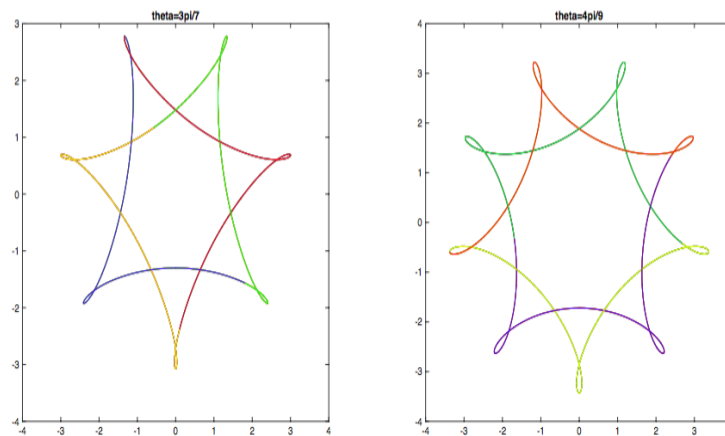
Figure 4.3.3: T=100 N=20 of the simple choreographic of 4 bodies chase each other. Left : $\theta = \frac{3\pi}{7}$, error of the Hamiltonian is 2.6645×10^{-15}. Right: $\theta = \frac{4\pi}{9}$, error of the Hamiltonian is 1.9984×10^{-15}.
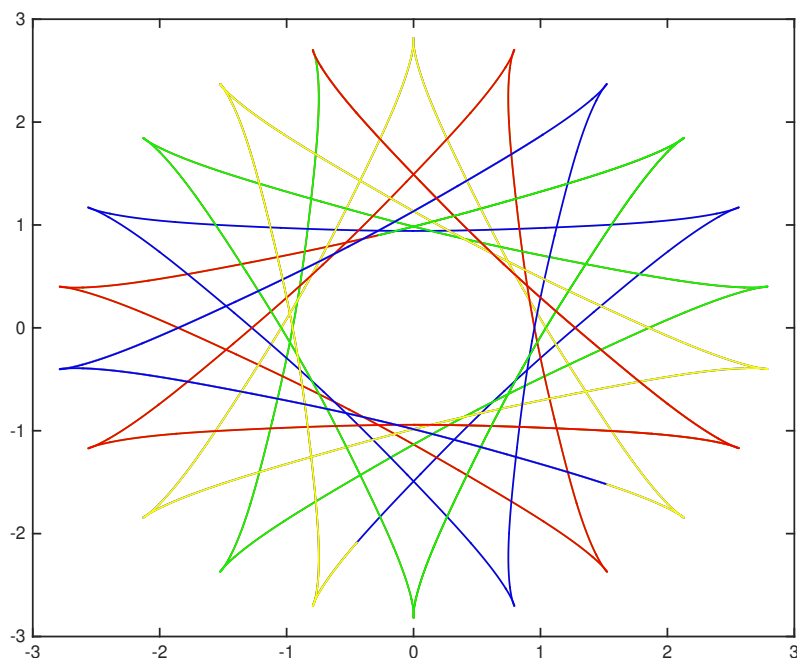
Figure 4.3.4: T=100 of the double-choreographic periodic solutions of $\theta = \frac{9\pi}{22}$, error of the Hamiltonian is 1.3323×10^{-15} with $N = 20$

4.3.2   Double-choreographic periodic orbits

The following definition can be found in [46].

Definition 4.3.1. *If the orbit of a periodic solution consists of two closed curves, then it is called a double-choreographic solution.*

Figure 4.3.4 shows a computed double-choreographic solution to 4-body problem using a spectral-Galerkin method.
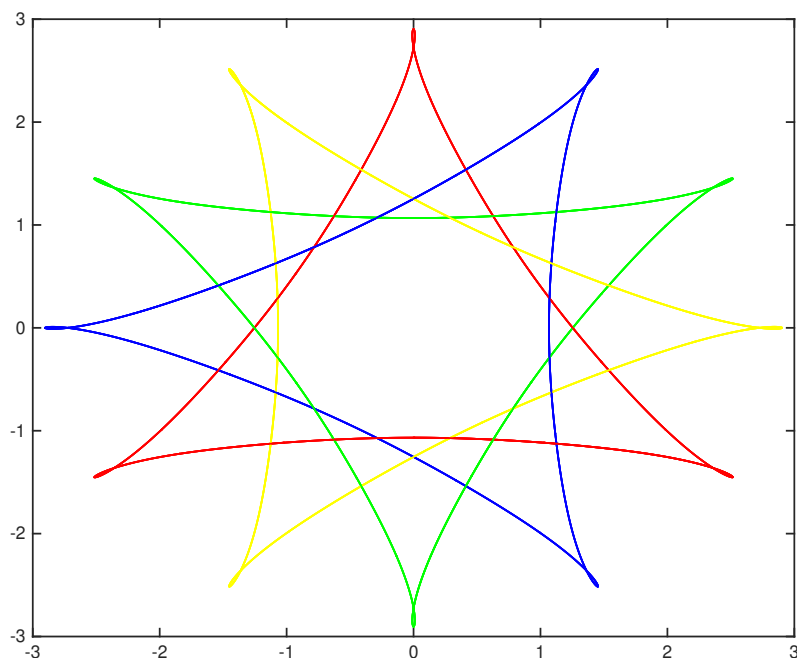
Figure 4.3.5: T=100 of the non-choreographic periodic solutions of $\theta = \frac{5\pi}{12}$ in [46], error of the Hamiltonian is 1.5543×10^{-15} with $N = 20$

4.3.3 Non-choreographic periodic orbits

Definition 4.3.2. *If the orbit of a periodic solution consists of different closed curves, it called a non-choreographic solution to emphasize that each closed curve is the trajectory of exact one body.*

Computational results are shown in Figure 4.3.5, illustrating a non-choreographic solution.

CHAPTER 5   APPLICATION II: APPROXIMATION FOR WEYL'S LAW

In quantum mechanics, Hamiltonian H become Schrodinger operator

$$\hat{H} = -\Delta + V$$

Considering the eigenvalue problems $\hat{H}\psi = \lambda\psi$, we denote a counting function $N(\lambda) = \#\{m : \lambda_m < \lambda\}$ (i.e., the number of eigenvalues smaller than λ), which is called the integrated density of states (IDOS) for Schrödinger operator. Arnold etc al ([47]) generalized the Weyl's Law from Laplacian operator (section 4.1 on page 612 of [48]) to Schrödinger operator : IDOS can be approximated by the volume (normalized) in the phase space (x, k) that can be explored by a classical of mechanical energy smaller than λ:

$$N(\lambda) \propto N_V = \frac{1}{(2\pi)^d} \iint_{k^2 + V(x) \leq \lambda} dxdk \tag{5.0.1}$$

Remark. The phase space is defined through Fourier transform $D^{\hat{\alpha}}\phi(\xi) = \xi^{\alpha}\hat{\phi}(\xi)$

However, Weyl's formula is only valid in the asymptotic limit $\lambda \to +\infty$ and can be very inaccurate at lower energies.

5.1   Effective Confine Potential

Arnold etc.al in [47] provided an effective confining potential $W = 1/u$ to be a remarkable approximation of the states for a large variety of one-dimensional systems, periodic or random, where the landscape u is defined as the solution of

$$-\Delta u + Vu = 1 \tag{5.1.1}$$

with certain boundary condition. [47] used this effective confining potential W to replace the original discrete random potential V and got a better approximation N_W. The reason of such an effective confining potential W works is roughly explained in

[47] without exact mathematical proof.

For Schrödinger eigenvalue problem $-\Delta\phi + V\phi = \lambda\phi$. One writes $\phi = u\varphi$ where u is landscape defined before. Using $\Delta(u\varphi) = u\Delta\varphi + 2\nabla u \cdot \nabla\varphi + \varphi\Delta u$, one obtain:

$$-\Delta\varphi - 2\frac{\nabla u}{u} \cdot \nabla\varphi + \frac{1}{u}\varphi = \lambda\varphi \tag{5.1.2}$$

And by

$$
\begin{aligned}
div(u^2\nabla\varphi) &= \nabla(u^2) \cdot \nabla\varphi + u^2 div(\nabla\varphi) \\
&= 2u\nabla u \cdot \nabla\varphi + u^2\Delta\varphi
\end{aligned}
\tag{5.1.3}
$$

Then the auxiliary function $\varphi = \phi/u$ obeys a following Schrödinger-type equation in which the original potential V has disappeared. Instead, a new function W now plays the role of effective confining potential. From [47], W continuously simulates the behavior of V well.

$$-\frac{1}{u^2}div(u^2\nabla\varphi) + W\varphi = \lambda\varphi \tag{5.1.4}$$

In this procedure, solving (5.1.1) in high precision to get landscape u is one of the most important step. We will use spectral method to solve (5.1.1) when V is an inverse square potential on a disk in Dirichlet boundary condition.

5.2 Approximation for Inverse Square Potential on Disk in Dirichlet Condition

We use this effective confining potential construction method to eliminate the singularity of the inverse square potential at the origin and reach a better approximation. We consider eigenvalue problems on a disk of radius R with Dirichlet boundary condition.

$$
\begin{aligned}
-\Delta\phi + \frac{c^2}{|x|^2}\phi &= \lambda\phi \quad in \quad D(0, R) \\
\phi &= 0 \quad on \quad \partial D(0, R)
\end{aligned}
\tag{5.2.1}
$$

c=1/2	$\lambda_1 = 9.8696$	$\lambda_2 = 15.9205$	$\lambda_3 = 27.1817$	$\lambda_4 = 39.4784$	$\lambda_5 = 41.3549$
c=2/3	$\lambda_1 = 11.3947$	$\lambda_2 = 16.8234$	$\lambda_3 = 27.7998$	$\lambda_4 = 41.8561$	$\lambda_5 = 42.6442$
c=100	$\lambda_1 = 11845$	$\lambda_2 = 11846$	$\lambda_3 = 11850$	$\lambda_4 = 11855$	$\lambda_5 = 11863$

Table 5.2.1: First 5 eigenvalues corresponding to different c. From [49] and [50], we have $c^2 < \lambda_1 < (c+1)(\sqrt{c+2}+1)^2$.

In polar coordinates, the Laplace operator can be written as

$$\Delta = \frac{\partial^2}{\partial r^2} + \frac{1}{r}\frac{\partial}{\partial r} + \frac{1}{r^2}\frac{\partial^2}{\partial \theta^2}$$

which leads to variable separation and the explicit representation of eignfunctions $\phi_{nk1} = J_{\nu_n}(\sqrt{\lambda_{n,k}}r)\cos n\theta$ and $\phi_{nk2} = J_{\nu_n}(\sqrt{\lambda_{n,k}}r)\sin n\theta$, where J_{ν_n} is the first kind of Bessel function of real order $\nu_n = \sqrt{n^2 + c^2}$. And set by Dirichlet boundary condition, we can get eigenvalues $\lambda_{n,k}$.

$$J_{\nu_n}(\sqrt{\lambda_{n,k}}R) = 0 \qquad (5.2.2)$$

For each $n = 0, 1, 2, ...$, this equation has infinitely many eigenvalues $\lambda_{n,k}$ which are enumerated by the index $k = 1, 2, 3, ...$ The eigenvalues interlace as $\lambda_{n,k} < \lambda_{n+1,k} < \lambda_{n,k+1} < \lambda_{n+1,k+1}$ from the properties of zeros of Bessel function. Therefore, we can determine mth eigenvalue by arranging $\lambda_{n,k}$ for $0 \leq n \leq m-1$ and $1 \leq k \leq m$ (See Table 5.2.1 for $m = 5$). Thus we can get $N(\lambda)$ accurately. And it follows from Weyl's formula that $N_V(\lambda) = (2\pi)^{-d}\iint_{k^2+V(x)\leq\lambda} dxdk$ can be derived explicitly.

$$\begin{aligned}
N_V(\lambda) &= \frac{1}{4\pi^2}\iint_{k^2+\frac{c^2}{|x|^2}\leq\lambda} d^2x\,d^2k \\
&= \frac{1}{4\pi^2}\iint_{|k|\leq\sqrt{\lambda-\frac{c^2}{|x|^2}}} d^2k\,d^2x \\
&= \frac{1}{4\pi^2}\int_{\frac{c^2}{|x|^2}\leq\lambda}\pi(\lambda - \frac{c^2}{|x|^2})d^2x
\end{aligned} \qquad (5.2.3)$$

Therefore

$$N_V(\lambda) = \begin{cases} \frac{1}{2}[\frac{\lambda}{2}(1 - \frac{c^2}{\lambda}) + c^2 \ln \frac{c}{\sqrt{\lambda}}] & \lambda \geq c^2 \\\\ 0 & \lambda \leq c^2 \end{cases}$$

We now compute a new approximation of the counting function $N(\lambda)$ based on the the effective confining potential $W = 1/u$. where landscape u is the solution of $-\Delta u + \frac{c^2}{|x|^2}u = 1$ on a unit disk D with Dirichlet boundary condition.

5.3 Spectral-Galerkin Method for Solving Landscape

We use Spectral-Galerkin method II in [51] as following : We try to find the radial solution $u_K(r) \in V_K = \{P_k : 1 \leq k \leq K\}$ such that for any $v \in V_K$,

$$(\nabla u_K, \nabla v)_D + c^2(u_K, v)_{r^{-2}, D} = (1, v)_D$$

where $P_k(r) = \frac{2k+c}{k+c} J_k^{-1,c}(2r^2 - 1)r^c$, $J_k^{-1,c}$ is generalized Jacobi polynomials defined in [51] that $J_k^{-1,c}(z) = \frac{(k+c)(z-1)}{2k} J_{k-1}^{1,c}(z)$. By Lemma 3.2 in [51] we have

$$(\nabla P_k, \nabla P_j)_D + c^2(P_k, P_j)_{r^{-2}, D} = 4\pi \delta_{k,j}(2k + c)$$

And

$$\begin{aligned} (1, P_j)_D &= \frac{2\pi(2j + c)}{j + c} \int_0^1 J_j^{-1,c}(2r^2 - 1)r^{c+1}dr \\\\ &= \frac{\pi(2j + c)}{2^{\frac{c+2}{2}}(j + c)} \int_{-1}^1 J_j^{-1,c}(z)(z + 1)^{\frac{c}{2}}dz \\\\ &= \frac{\pi(2j + c)}{2^{\frac{c+2}{2}}(j + c)} \int_{-1}^1 [J_j^{0,c}(z) - J_{j-1}^{0,c}(z)](z + 1)^{\frac{c}{2}}dz \end{aligned} \qquad (5.3.1)$$

By explicit formula (7.32) in page 63 of [52],

$J_j^{0,c}(z) = \sum_n^j a_{n=0}^j J_n^{0,\frac{c}{2}}(z)$ and $J_j^{0,c}(z) = \sum_{n=0}^{j-1} a_n^{j-1} J_n^{0,\frac{c}{2}}(z)$ We write 1 as $J_0^{0,\frac{c}{2}}(z)$, then
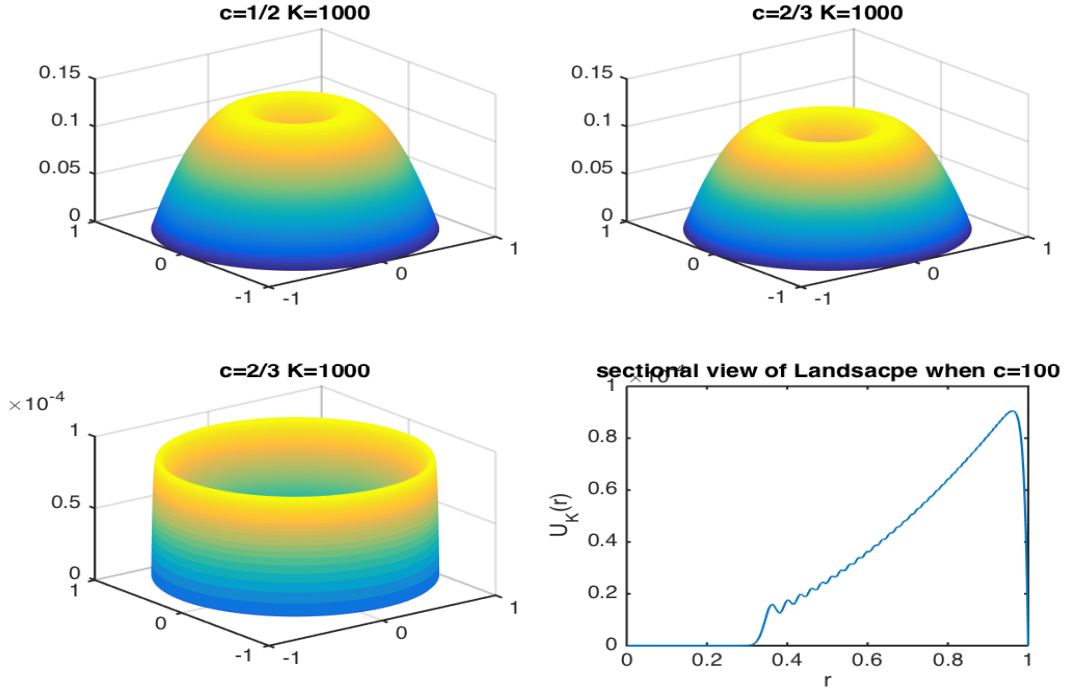
Figure 5.3.1: The height of landscape will decrease when c increases because $u_K(r) \sim O(c^{-2})$. And it also appears localization.

by the orthogonal property of Jaccobi polynomials

$$\int_{-1}^{1}[\sum_{n=1}^{j} a_n^j J_n^{0,\frac{c}{2}}(z) - \sum_{n=1}^{j-1} a_n^{j-1} J_n^{0,\frac{c}{2}}(z)](z+1)^{\frac{c}{2}} J_0^{0,\frac{c}{2}} dz = \frac{2^{\frac{c}{2}+1}}{\frac{c}{2}+1}(a_0^j - a_0^{j-1})$$

So

$$
\begin{aligned}
(1,P_j)_D &= \frac{\pi(2j+c)}{(j+c)(\frac{c}{2}+1)}[\frac{(-1)^j(\frac{c}{2})_j}{(\frac{c}{2}+2)_j} - \frac{(-1)^{j-1}(\frac{c}{2})_{j-1}}{(\frac{c}{2}+2)_{j-1}}] \\
&= \frac{(-1)^j c\pi(2j+c)^2}{2(j+c)(\frac{c}{2}+k-1)(\frac{c}{2}+k)(\frac{c}{2}+k+1)}
\end{aligned}
$$

(5.3.2)

Therefore we get the explicit expression of the numerical solution (See Figure 5.3.1)

$$u_K(r) = cr^c(r^2-1)\sum_{k=1}^{K} \frac{(-1)^k J_{k-1}^{1,c}(2r^2-1)}{(c+2k-2)(c+2k)(c+2k+2)}$$

After getting the numerical expression of $W = 1/u_k$, then we plugged $V = W$ in

$N_V(\lambda)$ so that

$$\begin{aligned}
N_W(\lambda) &= \frac{1}{4\pi^2} \iint_{k^2 + \frac{1}{u_K(|x|)} \leq \lambda} d^2x\, d^2k \\
&= \frac{1}{4\pi^2} \iint_{|k| \leq \sqrt{\lambda - \frac{1}{u_K(|x|)}}} d^2k\, d^2x \\
&= \frac{1}{4\pi^2} \int_{\frac{1}{u_K(|x|)} \leq \lambda} \pi\left(\lambda - \frac{1}{u_K(|x|)}\right) d^2x \qquad (5.3.3) \\
&= \frac{1}{2} \int_{u_K(r) > \frac{1}{\lambda}} \left(\lambda - \frac{1}{u_K(r)}\right) r\, dr \\
&= \frac{1}{2} \int_0^1 F(r)\, dr
\end{aligned}$$

where

$$F(r) = \begin{cases} \left(\lambda - \frac{1}{u_K(r)}\right) r & u_K(r) > \frac{1}{\lambda} \\ \\ 0 & u_K(r) \leq \frac{1}{\lambda} \end{cases}$$

Then we use Gauss-Legendre Rule to compute integral part of $N_W(\lambda)$ for given λ (for example 10 points and 100 or 1000 equally spaced nodes). See figure 5.3.2 for the N_W compared with N_V for approximation of $N(\lambda)$. Weyl's Law gives a upper bound approximation and the effective coffining potential provides a lower bound.
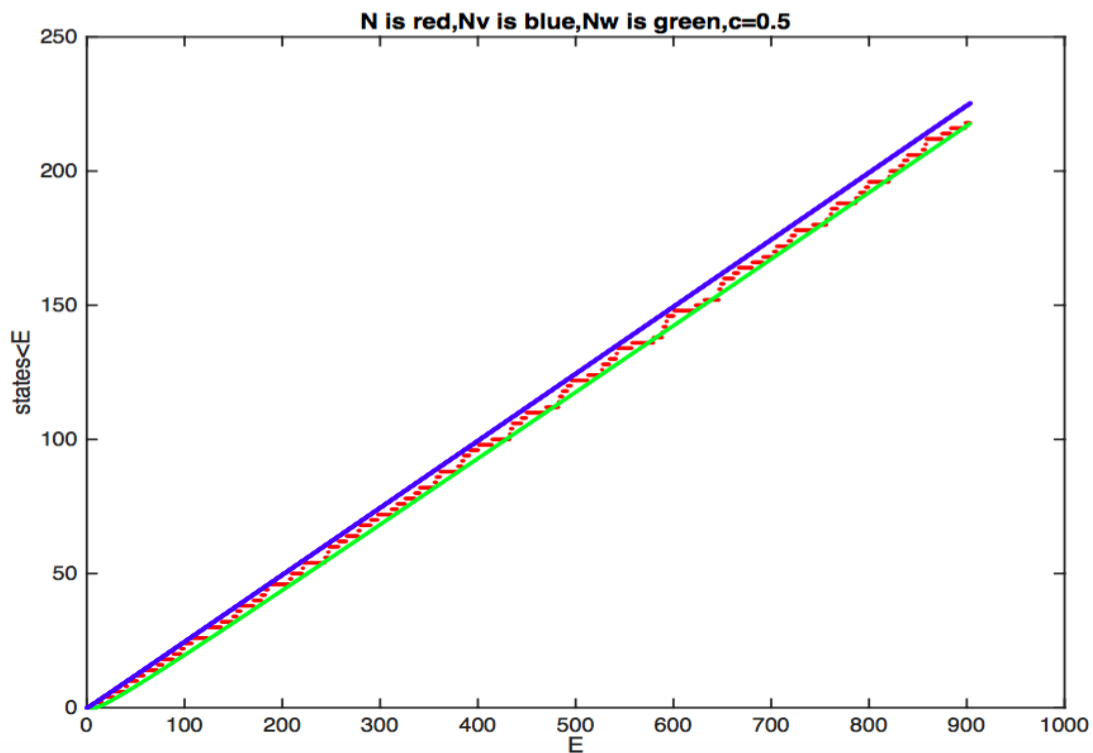
Figure 5.3.2: For inverse square potential, the counting function N (the red line)is the presented, together with N_V (the blue line) , Weyl's approximation using the original potential $V = c^2/r^2$, and N_W (the green line), the same with effective confining potential W. Notice the more remarkable agreement between N and N_W

CHAPTER 6   APPLICATION III: DISSIPATIVE DYNAMICS OF HAMILTONIAN SYSTEM

The work in this chapter is cooperate with Dr.Jing An and Dr.Wenzhao Zhang ([53]) , we use a typical example in quantum mechanics to show the application of our method. As shown in figure 6.0.1, we consider a standard model of an optomechanical system in which the cavity mode is driven by a laser coupled to the mechanical resonator via radiation pressure.

The Hamiltonian reads ($\hbar = 1$):

$$\mathbf{H} = \mathbf{H}_{sys} + \mathbf{H}_d, \tag{6.0.1}$$

$$\mathbf{H}_{sys} = \omega_c \mathbf{a}^\dagger \mathbf{a} + \omega_m \mathbf{b}^\dagger \mathbf{b} - g\mathbf{a}^\dagger \mathbf{a}(\mathbf{b}^\dagger + \mathbf{b}), \tag{6.0.2}$$

$$\mathbf{H}_d = \epsilon(\mathbf{a}^\dagger e^{-i\omega_d t} + \mathbf{a} e^{i\omega_d t}), \tag{6.0.3}$$

where $\mathbf{a}$ and $\mathbf{b}$ are the bosonic operators for the optical and mechanical modes with frequencies ω_c and ω_m respectively, $\mathbf{a}^\dagger$ denotes the Hermite transpose of $\mathbf{a}$, g is the single-photon coupling coefficient of the optomechanical interaction and $\mathbf{H}_d$ describes the standard continuous-wave drive; ω_d is the angular frequency of the laser and ϵ is the cavity driving strength given by $\epsilon \equiv 2\sqrt{P\kappa_{ex}/(\hbar\omega_d)}$, with P being the input power of the laser and κ_{ex} being the input rate of the cavity.

By rewriting the quantum Langevin equations a as a classical nonlinear equations
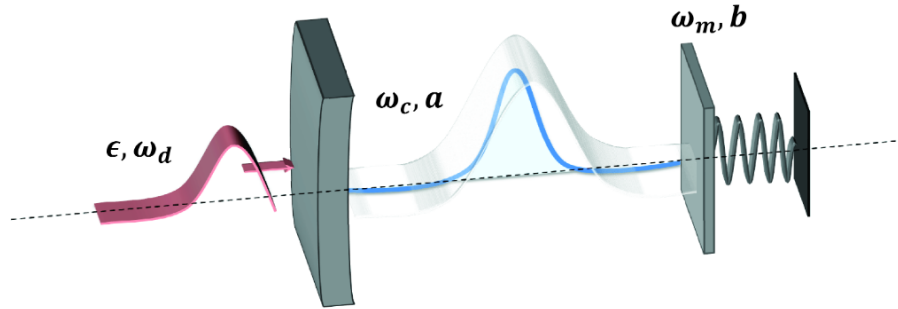
Figure 6.0.1: Sketch of a typical optomechanical system.

coupled to linearized quantum equations ([53]), the differential equations are given by

$$\frac{d\alpha}{dt} = -(i\delta + \kappa/2)\alpha + ig\alpha(\beta + \beta^*) - i\epsilon, \tag{6.0.4}$$

$$\frac{d\beta}{dt} = -(i\omega_m + \gamma/2)\beta + ig|\alpha|^2, \tag{6.0.5}$$

and

$$\frac{dN_a}{dt} = -\kappa N_a - iG^*(\langle \mathbf{a_1 b_1} \rangle + \langle \mathbf{a_1^\dagger b_1} \rangle^*) + iG(\langle \mathbf{a_1^\dagger b_1} \rangle + \langle \mathbf{a_1 b_1} \rangle^*), \tag{6.0.6}$$

$$\frac{dN_b}{dt} = -\gamma N_b + 2\gamma n_{th} - i(G\langle \mathbf{a_1^\dagger b_1} \rangle + G^*\langle \mathbf{a_1 b_1} \rangle - G\langle \mathbf{a_1 b_1} \rangle^* - G^*\langle \mathbf{a_1^\dagger b_1} \rangle^*), \tag{6.0.7}$$

$$\frac{d\langle \mathbf{a_1^\dagger b_1} \rangle}{dt} = -[i(\omega_m - \delta') + \frac{\kappa + \gamma}{2}]\langle \mathbf{a_1^\dagger b_1} \rangle - i(G^*\langle \mathbf{b_1^2} \rangle + G^* N_b - G\langle \mathbf{a_1^2} \rangle^* - G^* N_a),$$

$$\tag{6.0.8}$$

$$\frac{d\langle \mathbf{a_1 b_1} \rangle}{dt} = -[i(\omega_m + \delta') + \frac{\kappa + \gamma}{2}]\langle \mathbf{a_1 b_1} \rangle + i(G\langle \mathbf{b_1^2} \rangle + GN_b + GN_a + G + G^*\langle \mathbf{a_1^2} \rangle),$$

$$\tag{6.0.9}$$

$$\frac{d\langle \mathbf{a_1^2} \rangle}{dt} = -(2i\delta' + \kappa)\langle \mathbf{a_1^2} \rangle + 2iG(\langle \mathbf{a_1 b_1} \rangle + \langle \mathbf{a_1^\dagger b_1} \rangle^*), \tag{6.0.10}$$

$$\frac{d\langle \mathbf{b_1^2} \rangle}{dt} = -(2i\omega_m + \gamma)\langle \mathbf{b_1^2} \rangle + 2i(G^*\langle \mathbf{a_1 b_1} \rangle + G\langle \mathbf{a_1^\dagger b_1} \rangle), \tag{6.0.11}$$

where $N_a = \langle \mathbf{a_1^+ a_1} \rangle$, $N_b = \langle \mathbf{b_1^+ b_1} \rangle$, $\langle \mathbf{a_1^+ b_1} \rangle$, $\langle \mathbf{a_1 b_1} \rangle$, $\langle \mathbf{a_1^2} \rangle$, $\langle \mathbf{b_1^2} \rangle$ are the mean values of all the second-order moments. By solving the above equations, we can get the dynamic evolution of the optical mechanical system under the classical drive which can be used to explore the side-band cooling of the optical mechanical oscillator. Then by the algorithm described in 3.2.1 (detail can be found in [53]), we set up the following

iterative scheme:

$$\frac{2}{r}(\frac{du_{1N}^{k+1}}{dx}, \tilde{u}_{1N}) = -\frac{\kappa}{2}(u_{1N}^{k+1}, \tilde{u}_{1N}) + (\delta - 2g\beta_{1n})(u_{2N}^{k+1}, \tilde{u}_{1N})$$

$$- 2g\alpha_{2n}(s_{1N}^{k+1}, \tilde{u}_{1N}) + (-2gu_{2N}^k s_{1N}^k + c_{1n}, \tilde{u}_{1N}), \qquad (6.0.12)$$

$$\frac{2}{r}(\frac{du_{2N}^{k+1}}{dx}, \tilde{u}_{2N}) = (-\delta + 2g\beta_{1n})(u_{1N}^{k+1}, \tilde{u}_{2N}) - \frac{\kappa}{2}(u_{2N}^{k+1}, \tilde{u}_{2N})$$

$$+ 2g\alpha_{1n}(s_{1N}^{k+1}, \tilde{u}_{2N}) + (2gu_{1N}^k s_{1N}^k + c_{2n}, \tilde{u}_{2N}), \qquad (6.0.13)$$

$$\frac{2}{r}(\frac{ds_{1N}^{k+1}}{dx}, \tilde{s}_{1N}) = -\frac{\gamma}{2}(s_{1N}^{k+1}, \tilde{s}_{1N}) + \omega_m(s_{2N}^{k+1}, \tilde{s}_{1N}) + c_{3n}(1, \tilde{s}_{1N}), \qquad (6.0.14)$$

$$\frac{2}{r}(\frac{ds_{2N}^{k+1}}{dx}, \tilde{s}_{2N}) = 2g\alpha_{1n}(u_{1N}^{k+1}, \tilde{s}_{2N}) + 2g\alpha_{2n}(u_{2N}^{k+1}, \tilde{s}_{2N}) - \omega_m(s_{1N}^{k+1}, \tilde{s}_{2N})$$

$$- \frac{\gamma}{2}(s_{2N}^{k+1}, \tilde{s}_{2N}) + (g(u_{1N}^k)^2 + g(u_{2N}^k)^2 + c_{4n}, \tilde{s}_{2N}). \qquad (6.0.15)$$

and find $\mathbf{u}_N \in \mathbf{H}_N(I)$, such that

$$\frac{2}{r}(\frac{d\mathbf{u}_N}{dx}, \mathbf{v}_N) = (\mathcal{M}\mathbf{u}_N, \mathbf{v}_N) + (\mathcal{M}\mathbf{y}_n + \mathbf{f}, \mathbf{v}_N), \forall\ \mathbf{v}_N \in \mathbf{H}_N(I). \qquad (6.0.16)$$

6.1   Efficient implementation of the algorithm

When dealing with the iterative scheme (6.0.12) to (6.0.15),

Let

$$u_{1N}^{k+1} = \sum_{i=0}^{N-1} u_{1,i}^{k+1}\varphi_i, u_{2N}^{k+1} = \sum_{i=0}^{N-1} u_{2,i}^{k+1}\varphi_i, \qquad (6.1.1)$$

$$s_{1N}^{k+1} = \sum_{i=0}^{N-1} s_{1,i}^{k+1}\varphi_i, s_{2N}^{k+1} = \sum_{i=0}^{N-1} s_{2,i}^{k+1}\varphi_i. \qquad (6.1.2)$$

where the basis function φ is defined in (3.2.6).

Now, plugging the expression of (6.1.1) and (6.1.2) in (6.0.12)-(6.0.15) , and taking $\tilde{u}_{1N}, \tilde{u}_{2N}, \tilde{s}_{1N}, \tilde{s}_{2N}$ through all the basis functions in X_N, respectively, we will arrive at the following algebra system:

$$\mathcal{A}_n U_n^{k+1} = F_n^k, \qquad (6.1.3)$$

where

$$\mathcal{A}_n = \begin{pmatrix} \frac{2}{r}A + \frac{k}{2}M & -(\delta - 2g\beta_{1n})M & 2g\alpha_{2n}M & 0 \\ (\delta - 2g\beta_{1n})M & \frac{2}{r}A + \frac{k}{2}M & -2g\alpha_{1n}M & 0 \\ 0 & 0 & \frac{2}{r}A + \frac{\gamma}{2}M & -\omega_m M \\ -2g\alpha_{1n}M & -2g\alpha_{2n}M & \omega_m M & \frac{2}{r}A + \frac{\gamma}{2}M \end{pmatrix},$$

$$A = (s_{ij}), M = (m_{ij}), U_n^{k+1} = (u_{1,0}^{k+1}, \cdots, u_{2,N-1}^{k+1} s_{1,0}^{k+1}, \cdots, s_{2,N-1}^{k+1})^T,$$

$$F_n^k = (f_{1,0}^k, \cdots, f_{1,N-1}^k, \cdots, f_{4,0}^k, \cdots, f_{4,N-1}^k)^T,$$

$$f_{1,i}^k = -2g(u_{2N}^k s_{1N}^k, \varphi_i) + c_{1n}(1, \varphi_i), f_{2,i}^k = 2g(u_{1N}^k s_{1N}^k, \varphi_i) + c_{2n}(1, \varphi_i),$$

$$f_{3,i}^k = c_{3n}(1, \varphi_i), f_{4,i}^k = g((u_{1N}^k)^2 + (u_{2N}^k)^2, \varphi_i) + c_{4n}(1, \varphi_i).$$

Similarly, let

$$\mathbf{u}_N = \sum_{i=0}^{N-1} (u_{1,i}, u_{2,i}, \cdots, u_{10,i})^T \varphi_i. \tag{6.1.4}$$

Now, plugging the expression of (6.1.4) in (6.0.16), and taking $\mathbf{v}_N$ through all the basis functions in P_{N-1}^{10}, we will arrive at the following algebra system:

$$\mathcal{B}_n U_n = F_n. \tag{6.1.5}$$

6.2 Numerical experiments

We now perform a numerical test to study the convergence behavior and show the effectiveness of our algorithm. We operate our programs in MATLAB 2015b and take $\delta = 1, \omega_m = 1, \gamma = 10^{-5}, \kappa = 10^{-2}, g = 10^{-4}, \varepsilon = 50$ and $\alpha_1(0) = 100, \alpha_2(0) = 0, \beta_1(0) = 100, \beta_2(0) = 0$, $\mathbf{y}(0) = [0\ 100\ 0\ 0\ 0\ 0\ 0\ 0\ 0\ 0]$ as an example. In order to verify the validity of our method in the study of the system's behavior, we compare
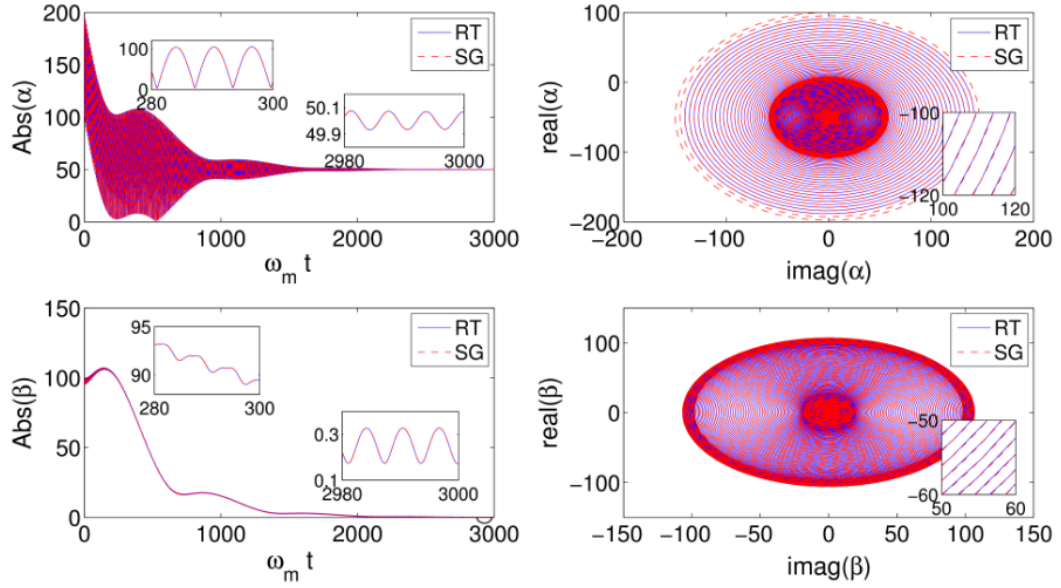
Figure 6.2.1: Time evolution and phase space diagram for the mean value α and β. The blue-solid line denotes the fourth-order Runge-Kutta method. The red-dashed line denotes the spectral-Galerkin method. $\delta/\omega_m = 1$, $\gamma/\omega_m = 10^{-5}$, $\kappa/\omega_m = 10^{-2}$, $g/\omega_m = 10^{-4}$, $\varepsilon/\omega_m = 50$ and $\alpha_1(0) = 100$, $\alpha_2(0) = 0$, $\beta_1(0) = 100$, $\beta_2(0) = 0$.

the commonly used fourth-order Runge-Kutta method in the drawing of dynamical evolution and phase space diagram in figure 6.2.1. It is obvious that these two methods match well, either in the overall trend or in the local details (subgraphs). Thus, our method can be used to describe the dynamical evolution of the system.

We compare the CPU times with the spectral Galerkin method and fourth order Runge-Kutta method. The CPU times for each method are shown in Table 6.2.1. We

Table 6.2.1: Comparison of CPU times between two methods for $y_2(t)$.

Methods	time(secs)	Error
Spectral Galerkin, N=20 on [0,10000]	51.85	1.00×10^{-15}
Spectral Galerkin, N=10 on [0,1000]	6.59	2.75×10^{-11}
Runge-Kutta method 4th order $h = 0.01$ on [0,10000]	981.82	3.98×10^{-5}
Runge-Kutta method 4th order $h = 0.01$ on [0,1000]	95.99	3.87×10^{-2}

Table 6.2.2: The numerical results of $\alpha_1(t)$ at different nodes for different N.

N	$t = 10$	$t = 100$	$t = 1000$	$t = 10000$
10	-166.587440305085	34.659101340286	-41.83989644877729	-50.00125015872428
15	-166.587440305224	34.659101340700	-41.83989644868462	-50.00125015872425
20	-166.587440305224	34.659101340699	-41.83989644868906	-50.00125015872424
25	-166.587440305224	34.659101340697	-41.83989644868994	-50.00125015872424

Table 6.2.3: The numerical results of $\alpha_2(t)$ at different nodes for different N.

N	$t = 10$	$t = 100$	$t = 1000$	$t = 10000$
10	82.1654738912417	10.2187420624481	3.645557496377773	-0.250018753909089
15	82.1654738908175	10.2187420630253	3.645557497121962	-0.250018753909113
20	82.1654738908164	10.2187420630310	3.645557497126441	-0.250018753909095
25	82.1654738908162	10.2187420630303	3.645557497125974	-0.250018753909120

know from Table 6.2.1 that the spectral Galerkin method is more effective in the long run. It takes less CPU time and obtains higher accuracy than fourth order Runge-Kutta method.

To better show the superiority of our method in accuracy, the numerical results of $\alpha_i(t), \beta_i(t), y_i(t), (i = 1, 2)$ at different nodes for different N are listed in Table 6.2.2-6.2.7.

We know from Table 6.2.2-6.2.7 that the approximate solutions of $\alpha_i(t), \beta_i(t), y_i(t), (i = 1, 2)$ achieve at least twelve-digit accuracy with $N \geq 20$.

In addition, the dynamics of cooling is also shown for two different methods in figure 6.2.2. Due to the convergence of the function to the stable value, there is no difference between the two methods in the stable time region (long time scale). In fact, we know

Table 6.2.4: The numerical results of $\beta_1(t)$ at different nodes for different N.

N	$t = 10$	$t = 100$	$t = 1000$	$t = 10000$
10	-75.4853411160147	105.7504327687671	6.329412203038785	0.250018751952199
15	-75.4853411161271	105.7504327693629	6.329412202374115	0.250018751952200
20	-75.4853411161273	105.7504327693617	6.329412202363541	0.250018751952201
25	-75.4853411161273	105.7504327693596	6.329412202362347	0.250018751952180

Table 6.2.5: The numerical results of $\beta_2(t)$ at different nodes for different N.

N	$t = 10$	$t = 100$	$t = 1000$	$t = 10000$
10	59.4843495594285	-4.0325727064729	14.150059714947194	0.000001248320982
15	59.4843495593981	-4.0325727056435	14.150059715927437	0.000001248320987
20	59.4843495593975	-4.0325727056375	14.150059715928842	0.000001248320989
25	59.4843495593975	-4.0325727056366	14.150059715926586	0.000001248320983

Table 6.2.6: The numerical results of $y_1(t)$ at different nodes for different N.

N	$t = 10$	$t = 100$	$t = 1000$	$t = 10000$
10	0.464551547681799	14.311649704842445	1.168716058184881	0.399228665114767
15	0.464551547743722	14.311649704880143	1.168716058163812	0.399228665114767
20	0.464551547743722	14.311649704880217	1.168716058163804	0.399228665114767
25	0.464551547743722	14.311649704880233	1.168716058163796	0.399228665114767

Table 6.2.7: The numerical results of $y_2(t)$ at different nodes for different N.

N	$t = 10$	$t = 100$	$t = 1000$	$t = 10000$
10	99.705531715317093	80.452359594261452	1.350409600121569	0.798842709265668
15	99.705531715382847	80.452359594191478	1.350409600094054	0.798842709265668
20	99.705531715382847	80.452359594191506	1.350409600094044	0.798842709265668
25	99.705531715382847	80.452359594191449	1.350409600094035	0.798842709265667
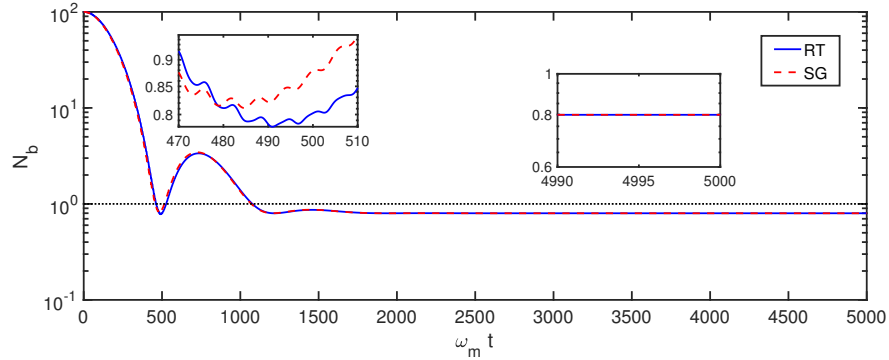
Figure 6.2.2: Dynamics of sideband cooling. The blue-solid line denotes the fourth order Runge-Kutta method. The red-dashed line denotes the spectral-Galerkin method. The initial condition $N_a(0) = 0$, $N_b(0) = 100$ and the thermal noise $n_{th} = 200$. Other parameters are the same as figure 2

from Table 6.2.1 that the spectral Galerkin method exhibits higher accuracy. In the case of the unstable evolution part, the details of the graph are invoked, especially in the inflection points as shown in the subgraph. And this unstable minimum value is usually used in modulation cooling .Thus, our method has greater advantages in the study of such problems.

CHAPTER 7   UPCOMING UNSOLVED PROBLEM : NONSMOOTH HAMILTONIAN SYSTEMS

7.1   Hamiltonian Systems with Dirac Delta Function

Kicked rotator is one of the most thoroughly studied chaotic systems, both classically and quantum mechanically ([54]). Its Hamiltonian is given by

$$H(t) = \frac{L^2}{2I} + k\cos\theta \sum_n \delta(t - nT) \tag{7.1.1}$$

The first term describes the rotation of a pendulum with angular momentum L, and a moment of inertial I. The second term describes periodic kicks with a period T by a pulsed gravitational potential of strength $k = mgh$. The kicked rotator belongs to Hamiltonian systems. The equations of motion are obtained from the canonical equations

$$\begin{cases} \dot\theta = \frac{\partial H}{\partial L}, \\[2mm] \dot L = -\frac{\partial H}{\partial \theta} \end{cases} \tag{7.1.2}$$

whence follows, with the Hamiltonian (7.1.1)

$$\begin{cases} \dot\theta = L \\[2mm] \dot L = k\sin\theta \sum_n \delta(t - n) \end{cases} \tag{7.1.3}$$

where now I and T have been normalized to 1.

This example convincingly demonstrates the superiority of theory over experiment. It is not so easy to realize such a situation experimentally. Therefore numerically simulation this example becomes very meaningful. The difficulty in the numerical methods is that L changes discontinuously.

7.2 Fractional Exponent Hamiltonian System

Considering Hamiltonian $H(p, q) = Ap^\alpha + Bq^\beta$, where $\alpha\beta \neq 0$ and $0 \leq t \leq 1$. Without lose generation, we may assume $A = B = 1$, since we can use scaling

$$\begin{cases} p = A^{-\frac{1}{\alpha}}\hat{p} \\ q = B^{-\frac{1}{\alpha}}\hat{q} \end{cases}$$

then we obtain the following Hamiltonian system

$$\begin{cases} \dot{p} = -\beta q^{\beta-1} \\ \dot{q} = \alpha p^{\alpha-1} \end{cases}$$

with initial value

$$\begin{cases} p(0) = p_0 \\ q(0) = q_0 \end{cases}$$

By theory of Hamiltonian system,

$$H(p(t), q(t)) = p(t)^\alpha + q(t)^\beta \equiv C \tag{7.2.1}$$

is an invariant for any time t.

When $\alpha, \beta \geq 2$, Lipschitz continuity can grantee the existence and uniqueness of the solution.

Some observations :

1. If $p_0, q_0 > 0$, $p(t)$ will decrease to 0 and its decrease speed will be faster and faster. $q(t)$ will increase and its increase speed will slower to 0.

2. If $H(0, 0) = p_0^\alpha + q_0^\beta = 0$. We assume solution are in the form of

$$\begin{cases} p(t) = p_0(1 - t)^{r_1} \\ q(t) = q_0(1 - t)^{r_2} \end{cases}$$

By substitution, we have

$$\begin{cases} r_1 = \dfrac{\beta}{\alpha + \beta - \alpha\beta} \\[3mm] r_2 = \dfrac{\alpha}{\alpha + \beta - \alpha\beta} \end{cases}$$

If r_1, r_2 are integers, it is the usual smooth Hamiltonian system. When r_1, r_2 are not integers, it dose not smooth as usual.

3. If $\alpha = \beta = 2$,

$$\begin{cases} p(t) = p_0 \cos 2t - q_0 \sin 2t \\[2mm] q(t) = q_0 \cos 2t + p_0 \sin 2t \end{cases}$$

Numerical Example Considering Hamiltonian $H(p, q) = \frac{5}{4}(q^2 - p^{\frac{6}{5}})$ and $0 \le t \le 1$

$$\begin{cases} \dot{p} = -\dfrac{5}{2}q \\[3mm] \dot{q} = -\dfrac{3}{2}p^{\frac{1}{5}} \end{cases}$$

with initial value

$$\begin{cases} p(0) = -1 \\[2mm] q(0) = -1 \end{cases}$$

The exact solution is

$$\begin{cases} p(t) = -\sqrt{(1-t)^5} \\[2mm] q(t) = -\sqrt{(1-t)^3} \end{cases}$$

which only reach the C^1 at $t = 1$

(a) Preprocess of the Equations

    i. Zero initialization : Let $\tilde{p} = p - p(0)$, $\tilde{q} = q - q(0)$.

    ii. Normalization: Let $t = \frac{x+1}{2}, x \in [-1, 1]$,

Then the equation is equivalent to solving the following nonlinear Hamilto-

nian systems:

$$\begin{cases} \dot{\tilde{p}} = -\dfrac{5}{4}(\tilde{q} + q(0)) \\ \dot{\tilde{q}} = -\dfrac{3}{4}(\tilde{p} + p(0))^{\frac{1}{5}} \end{cases}$$

(b) Weak Form of Hamiltonian Systems

We introduce the following usual Sobolev space:

$$H_E^1(I) := \{u : u \in H^1(I), u(-1) = 0\},$$

where $I = [-1, 1]$. Let $X_N = P_N \cap H_E^1(I)$. Then the weak form is :

Find $p_N, q_N \in X_N$ such that for all $\tilde{p}_N, \tilde{q}_N \in X_N$,

$$\begin{cases} (\dot{p}_N, \tilde{p}_N) = -\dfrac{5}{4}(q_N + q(0), \tilde{p}_N) \\ (\dot{q}_N, \tilde{q}_N) = -\dfrac{3}{4}((p_N + p(0))^{\frac{1}{5}}, \tilde{q}_N) \end{cases}$$

(c) Iterative Scheme

In order to solve this weak form, we set up the following iterative scheme:

$$\begin{cases} (\dot{p_N}^{k+1}, \tilde{p}_N) = -\dfrac{5}{4}(q_N^k + q(0), \tilde{p}_N) \\ (\dot{q_N}^{k+1}, \tilde{q}_N) = -\dfrac{3}{4}((p_N^k + p(0))^{\frac{1}{5}}, \tilde{q}_N) \end{cases}$$

(d) Efficient Implementation of the Algorithm

We use basis functions defined as (3.2.6) for X_N. Let $p_N^{k+1} = \sum_{i=0}^{N-1} p_i^{k+1} \varphi_i$ and $q_N^{k+1} = \sum_{i=0}^{N-1} q_i^{k+1} \varphi_i$ and plugging in iterative scheme , and taking $\tilde{p}_N, \tilde{q}_N$ through all the basis functions in X_N, respectively, we will arrive at the following matrix form system:

$$\mathcal{A} U^{k+1} = F^k, \tag{7.2.2}$$
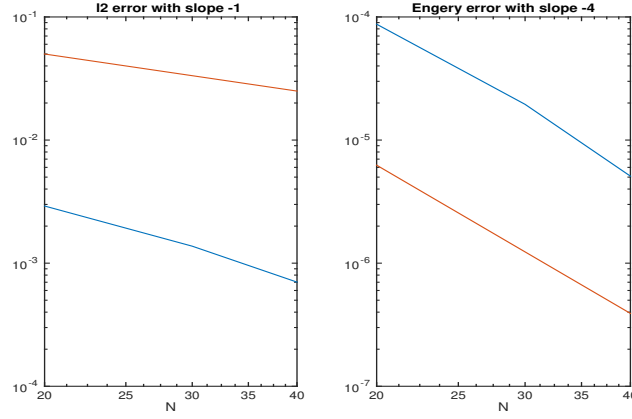
Figure 7.2.1: L_2 error and energy convergence rate at t=1 that are worse than usual smooth Hamiltonian system

where

$$\mathcal{A} = \begin{pmatrix} A & \frac{5}{4}M \\ 0 & A \end{pmatrix},$$

$$A = (s_{ij}), M = (m_{ij}), U^{k+1} = (p_0^{k+1}, \cdots, p_{N-1}^{k+1}, q_0^{k+1}, \cdots, q_{N-1}^{k+1})^T,$$

$$F_n^k = (f_{1,0}, \cdots, f_{1,N-1},, f_{2,0}^k, \cdots, f_{2,N-1}^k)^T,$$

$$f_{1,i} = -\frac{5}{4}(q(0), \varphi_i), f_{2,i}^k = -\frac{3}{4}((p_N^k + p(0))^{\frac{1}{5}}, \varphi_i).$$

In practice, we calculate the numerical integration by $P = 4N + 1$ Gauss points and tolerate condition as discrete norm $\|u_N^{k+1} - u_N^k\|_{L_2}^2 > 10^{-14}$ where $u_N = (p_N, q_N)$

(e) Numerical Result

Compared with the smooth Hamiltonian system examples computed in previous chapters and [36], the convergence rates of non-smooth Hamiltonian system are quite slow. These are seen in Figure 7.2.1.

CHAPTER 8   CONCLUSION

This work applies spectral methods to Hamiltonian systems. Two efficient pre-process strategies are proposed to provide a good initial value for the iterative schemes. one is using existed symplectic schemes to solve the system on a rough time step. The other one is to separate the system into linear part and nonlinear part. Then the solution to linear part is used as the initial value. By describing the high order derivative of Hamiltonian System with polynomial nonlinear part, we give the energy preserving error estimation of such type problems that the energy error is linearly accumulated. An numerical example about solving Henon-Heiles System is implement to verify this error estimation.

In the first application, we investigate the classical n-Body problems in $\mathbb{R}^2$. Several interesting orbits are simulated in high precision. For the second application, we approximate Weyl's law effectively by using spectral method to solve Landscape. In the last application, we proposed a new numerical method to solve the dynamics of a dissipative Hamiltonian system. Based on the spectral-Galerkin approximation, our method can achieve higher accuracy and shorter computation time compared with the fourth order Runge-Kutta method. Taking quantum optomechanical cooling as an example, we show the application of our method in quantum dissipative dynamics. In order to solve the nonlinear discrete scheme, we propose an iterative algorithm and construct an appropriate set of basis functions such that the matrices in the discrete variational form are sparse. Our scheme has obvious advantages in simulating dynamics that require long time evolution and high accuracy.

It's future work to design new spectral method to solve nonsmooth Hamiltonian system and divergence orbits of n-Body problems.

REFERENCES

[1] M. LEVI, *From Archimedes and Euclid to Hamilton and Poincare*, SIAM NEWS, December 2016.

[2] E. TRELAT AND E. ZUAZUA, *The turnpike property in finite-dimensional non-linear optimal control*, J.Differential Equations, vol.258(1), pp.81-114, (2015).

[3] F. CESCHINO AND J. KUNTZMANN, *Numerical Solutions of Initial Value Problems*, Prentice Hall, 1966.

[4] J.C. BUTCHER, *Implicit Runge-Kutta Processes*, Math.Comput., Vol.18(85), pp.50-64, (1964).

[5] E. HAIRER, S.P. NORESTT, AND G. WANNER, *Solving Ordinary Differential Equations I: Nonstiff Problems*, Springer Series in Computational Mathematics, Second Revised Edition, 1992.

[6] K. FENG, *On Difference Schemes and Symplectic Geometry*, Proceedings of the 5-th Intern, Symposium on Differential Geometry and Differential Equations, August 1984, Beijing.

[7] K. FENG, *Difference Schemes for Hamiltonian Formalism and Symplectic Geometry*, J.Comp.Math., Vol.4(3), pp.279-289, (1986).

[8] K. FENG, H. WU, M. QIN AND D. WANG, *Construction of Canonical Difference Schemes for Hamiltonian Formalism via Generating Functions*, J. Comp. Math., Vol.7(1), pp.71-96, (1989).

[9] K. FENG, *How to Compute Properly Newtons Equation of Motion?* Proceedings of the Second Conference on Numerical Methods for Partial Differential Equations, Nankai Univ., Tianjin, China, Eds. Ying Lungan & Guo Benyu, World Scientific, pp.15-22, (1991).

[10] K. FENG, *Formal Power Series and Numerical Algorithms for Dynamical systems*, Proceedings of International Conference on Scientific Computation, Hangzhou,

China, Eds. Tony Chan and Zhong-Ci Shi, Series on Appl. Math., Vol.1, pp.28-35, (1991).

[11] Y.B. Suris, *Hamiltonian Runge-Kutta Type Methods and Their Variational Formulation*, (In Russian), Mathematical Simulation, Vol.2, pp.78-87, (1990).

[12] J.M. Sanz-Serna, *The numerical integration of Hamiltonian systems*, Computational Ordinary Differential Equations, ed. by J.R. Cash & I. Gladwell, Clarendon Press, Oxford, pp.437-449, (1992).

[13] G. Sun, *Construction of high order symplectic Runge-Kutta Methods*, Comput. Math., Vol.11(3), pp.250-260, (1993).

[14] C. Chen, Q. Tong and S. Hu, *Finite Element Method with Superconvergence for Nonlinear Hamiltonian Systems*, Journal of Compuational Mathematics, Vol.29(2), pp.167-184, (2011).

[15] C. Canuto, M.Y. Hussaini, A. Quarteroni and T.A. Zang, *Spectral Methods in Fluid Dynamics*, Springer Series in Computational Physics, 1988.

[16] J. Shen, T. Tang and L-L. Wang, *Spectral Methods: Algorithms, Analysis and Applications*, Springer Series in Computational Mathematics, Springer, 2011.

[17] J. An, W. Cao and Z. Zhang, *A Class of Efficient Spectral Methods and Error Analysis for Nonlinear Hamiltonian Systems*, in preparation.

[18] V.I. Arnold, *Mathematical Methods of Classical Mechanics*, Springer, GTM 60, Second Edition, 1999.

[19] E. Hairer, C. Lubich and G. Wanner, *Geometric Numerical Integration:Structure-Preserving Algorithms for Ordinary Differential Equations*, Springer Series in Computational Mathematics, Second Edition, 2005.

[20] V.F. Lazuktin, *KAM Theory Semiclassical Approximations to Eigenfunctions*, Springer-Verlag, A Series of Mondern Surveys in Mathematics, 1991.

[21] J. Shen and J. Xu *Convergence and Error Analysis for the Scalar Auxiliary Variable (SAV) Schemes to Gradient Flows*, SIAM J. Numer. Anal., Vol.56(5), pp.2895-2912, (2018).

[22] J. Shen, J. Xu and J. Yang, *The Scalar Auxiliary Variable (SAV) Approach for Gradient Flows*, Journal of Compuational Physics, Vol.353, pp407-416, (2018).

[23] J. Shen, J. Xu and J. Yang, *A New Class of Efficient and Robust Energy Stable Schemes for Gradient Flows*, SIAM Rev, accepted (2019).

[24] L.C. Evans, *Partial Differential Equations*, Graduate Studies in Mathematics, Vol.19, American Mathematical Society.

[25] T. Brander, *Hamiton-Jacobi equations*, Master's Thesis, University of Jyvaskyla, 2012.

[26] T. Bjork, *Equilibrium Theory in Continuous Time*, Lecture Notes, Stockholm School of Economics, 2012.

[27] R. Kumar and H. Nasralah, *Portfolio Optimization Near Horizon*, arXiv:1611.09300v1, (2016).

[28] S. Nadtochiy and T. Zariphopoulou , *An Approximation Scheme for Solution to the Optimal Investment Problem in Incomplete Markets*, SIAM J. Financial. Math., Vol.4(1), pp.494-538, (2013).

[29] D. Liberzon and J. Lin, *Calculus of Variations and Optimal Control Theory: A Concise Introduction*, Lecture notes, UIUC, 2009.

[30] M. Falcone and R. Ferretti, *Numerical Methods for Hamilton-Jacobi Type Equations*, Handbook of Numerical Analysis, Vol.17, (2016).

[31] L.N. Trefethen, *Approximation Theory and Approximation Practice*, SIAM, 2013.

[32] Z. Zhang,*Superconvergence of Spectral Collocation and p-Version Methods in One Dimensional Problems*, Mathematics of Computation, Vol.74, pp.1621-1636,

(2005).

[33] Z. Zhang, *Superconvergence of a Chebyshev Spectral Collocation Method*, J. Sci. Comput., vol.34(3), pp.237-246, (2008).

[34] Y. Yang, Y. Huang and Y. Zhou, *Numerical Solutions for Solving Time Fractional Fokker-Planck Equations Based on Spectral Collocation Methods*, Journal of Computational and Applied Mathematics, vol.339, pp.389-404, (2017).

[35] L N. Trefethen, *Spectral Methods in MATLAB*, Tinghua University Press SIAM, 2011.

[36] N. Kanyamee and Z. Zhang, *Comparison of A Spectral collocation Method and Symplectic Methods for Hamiltonian Systems*, International Journal of Numerical Analysis and Modeling, Vol.8(1), pp.86-104, (2011).

[37] Y. Li, B. Wu and M. Leok, *Spectral-Collocation Variational Integrators*, Journal of Computational Physics, Vol.332, pp.83-98, (2017).

[38] R. Courant and D. Hilbert, *Methods of Mathematical Physics*, Volume I, Wiley Classics Edition Published in 1989.

[39] P.J. Davis and P. Rabinowitz, *Methods of Numerical Integration* , Dover Publications, Second Edition, 2007.

[40] H. Van de Vyver, *A fourth-order symplectic exponentially fitted integrator*, Computer Phys.Comm, Vol.174(4), pp.255-262, (2006).

[41] W. Kuang, T. Ouyang, Z. Xie and D. Yan, *The Broucke-Henon Orbit and the Schubart Orbit in the Planar Three-body Problem with Equal Masses*, arXiv preprint arXiv:1607.00580, (2016).

[42] C. Moore, *Braids in classical dynamics*, Phys.Rev.Lett, vol.70(24), pp.3675-3679, (1993).

[43] A. Chenciner and R. Montgomery, *A remarkable periodic solution of the 3-body problem in the case of equal masses*, Annals of Mathematics, Vol.152(3),

pp.881-901, (2000).

[44] T. KAPELA AND C. SIMO, *Computer assisted proofs for nonsymmetric planar choreographies and for stability of the Eight*, Nonlinearity, Vol.20(5), pp.1241-1255, (2007).

[45] G.E. ROBERTS, *Linear stability analysis of the figure-eight orbit in the three-body problem* , Ergodic Theory Dynam Systems, Vol.27(6), pp.1947-1963, (2007).

[46] T. OUYANG AND Z. XIE, *Star Pentagon Star and many stable choreographic solutions of Newtonian 4-body Problem*, Physica D, Vol.307, pp.61-76, (2015).

[47] D.N. ARNOLD, G. DAVID, D. JERISON AND M. FILOCHE, *Effective Confining Potential of Quantum States in Disordered Media*, Phys.Rev.Lett, Vol.116(5), 056602, (2015).

[48] D.S. GREBENKOV AND B.-T. NGUYEN, *Geometrical Structure of Laplacian Eigenfunctions*, SIAM Rev, Vol.55(4), pp.601-667, (2013).

[49] G.N. WATSON, *A Treatise on the Theory of Bessel Functions*, Cambridge At the University Press Second Edition, 1966.

[50] L.G. CHAMBERS *An upper bound for the first zero of Bessel functions* Math. Comput, Vol 38(15), pp.589-591, (1982).

[51] H. LI AND Z. ZHANG *Efficient Spectral and Spectral Element Methods for Eigenvalue Problems of Schrödinger Equations with an Inverse Square Potential*, SIAM Journal on Scientific Computing, Vol.39(1), pp.A114-A140, (2017).

[52] R. ASKEY *Orthogonal Polynomials and Special Functions*, SIAM 1975.

[53] J. AN, W. ZHANG AND L. ZHAO, *A high-precision numerical method for the dissipative dynamics of Hamiltonian systems*, submitted.

[54] H-J. STÖCKMANN, *Quantum Chaos : An Introduction*, Cambridge University Press, 1999.

ABSTRACT

SPECTRAL METHODS FOR HAMILTONIAN SYSTEMS
AND THEIR APPLICATIONS

by

LEWEI ZHAO

May 2019

Advisor: Dr. Zhimin Zhang

Major: Applied Mathematics

Degree: Doctor of Philosophy

Hamiltonian systems typically arise as models of conservative physical systems and have many applications. Our main emphasis is using spectral methods to preserve both symplectic structure and energy up to machine error in long time. An energy error estimation is given for a type of Hamiltonian systems with polynomial nonlinear part, which is numerical verified by solving a Henon-Heiles systems. Three interesting applications are presented : the first one is the n-body problems. The second one is approximation for Weyl's Law and the third one is simulating quantum cooling in an optomechanical system to study the dissipative dynamics. Moreover, nonsmooth Hamiltonian systems problems are discussed for the limitation of this method which motivates our future work.

AUTOBIOGRAPHICAL STATEMENT

Lewei Zhao

Education

- Ph.D. in Applied Mathematics, 2019
  Wayne State University, Detroit, Michigan, USA

- B.S. in Hongyi Mathematics Honors Class, 2014
  Wuhan University, Wuhan, China

Selected List of Awards and Scholarships

1. 2019/04, Award for Outstanding Achievement in PhD Program, Mathematics
   Department, Wayne State University.

2. 2018/06-08, Summer Dissertation Fellowship ($5000), Graduate School, Wayne
   State University.

3. 2016/04, Paul Caltin Endowed Mathematics Scholarship ($500), Mathematics
   Department, Wayne State University.

4. 2013/07, The 4th S.T.Yau College Mathematics Contest Honorable Mention in
   Applied and Computational Math Subject, China (Top 20).

Publications in Progress

1. J.AN, W.ZHANG AND L.ZHAO, *A High-precision Numerical Method for the Dissipative Dynamic of Hamiltonian System*, Submitted.

2. L.ZHAO, H.PAN AND Z.ZHANG, *Some New Developments of Polynomial Preserving Recovery on Hexagon Pattern and Chervon Pattern*, in preparation.